

the expression of GAPDH was simultaneously quantified using the following primers: 5'-CCTGGAGAAACCTGCCAAGTAT-3' and 5'-TGAA GTCGCAGGAGACAACCT-3'. The primers used to detect the AR were designed as described previously (Waza et al., 2005). The primers used for p62 detection were 5'-ATGCTGTCCATGGGTTTCTC-3' and 5'-GG TGGAGGGTGCTTTGAATA-3' for PC12 cells and 5'-CCAGTGATGA GGAGCTGACA-3' and 5'-CATCACAGATCACATTGGGG-3' for Neuro2A cells. The R.S.I. was computed as the signal intensity of each sample divided by the signal intensity of the control siRNA-transfected cells (see Fig. 3) and AR-24Q/p62<sup>(+/+)</sup> or AR-97Q/p62<sup>(+/+)</sup> mice (see Fig. 9).

**Statistical analyses.** The data were analyzed using unpaired *t* tests and *post hoc* tests (Tukey–Kramer tests) for multiple comparisons, along with the Kaplan–Meier and log-rank tests to assess the survival rate, as calculated using Statview software version 5 (Hulinks).

## Results

### AR is degraded via the p62-dependent autophagic pathway in cultured cells

p62 is degraded in the autophagic–lysosomal pathway through its interaction with LC3 (Komatsu et al., 2007; Ichimura et al., 2008). In addition, the AR can also be degraded by autophagy (Montie et al., 2009). To determine whether normal and mutant ARs are degraded by autophagy in cells in which the protein forms inclusions in the nucleus, as in motor neurons in SBMA, we treated an inducible PC12 cell model of SBMA that expresses full-length human AR with wild-type (AR-10Q) or mutant (AR-112Q) AR with bafilomycin A1, which is a potent inhibitor of autophagy. In this model, AR-112Q forms NIs in response to DHT, and treatment with DHT for 7 d increased the frequency of inclusions nearly threefold compared with treatment for 3 d (Walcott and Merry, 2002). Immunoblot analysis revealed a significant accumulation of monomeric wild-type (AR-10Q) and mutant (AR-112Q) AR in the PC12 cells that were treated with bafilomycin A1 after DHT treatment for 3 and 7 d; p62 also accumulated in the bafilomycin A1-treated cells (Fig. 1A). Bafilomycin A1 treatment also significantly increased the amount of the high-molecular-weight complex of mutant AR in the AR-112Q cells after DHT treatment for 7 d (Fig. 1A). Similar accumulations of AR-24Q, AR-97Q, and p62 were observed when we transiently transfected wild-type (AR-24Q) or mutant (AR-97Q) AR into Neuro2A cells and treated the cells with bafilomycin A1 (Fig. 1B). Accumulation of wild-type and mutant AR was similarly observed in treatment with lactacystin, which is a potent inhibitor of the ubiquitin–proteasome pathway (Fig. 1A,B). These findings suggest that the AR is degraded not only via the UPS but also via the autophagic–lysosomal pathway, and this effect occurs independently of inclusion formation in the nuclei. To examine whether AR was localized in LC3-positive cytoplasmic puncta, we cultured the PC12 cells with doxycycline, NGF, and DHT for 7 d. Immunofluorescence staining revealed that bafilomycin A1 treatment increased p62- and LC3-positive cytoplasmic puncta, which colocalized with both wild-type and mutant ARs (Fig. 1C). This result suggests that both wild-type and mutant ARs are degraded in the p62-dependent autophagic pathway. These findings are consistent with a previous study that reported that p62 interacted with mutant huntingtin and was degraded by autophagy (Bjørkøy et al., 2005). Nevertheless, p62 colocalized with AR-112Q in the NIs (Fig. 1C).

### p62 interacts with the AR

p62 interacts with LC3 via a short domain of its C-terminal portion and is selectively degraded by autophagy (Ichimura et al., 2008; Ichimura and Komatsu, 2010). However, it is unclear

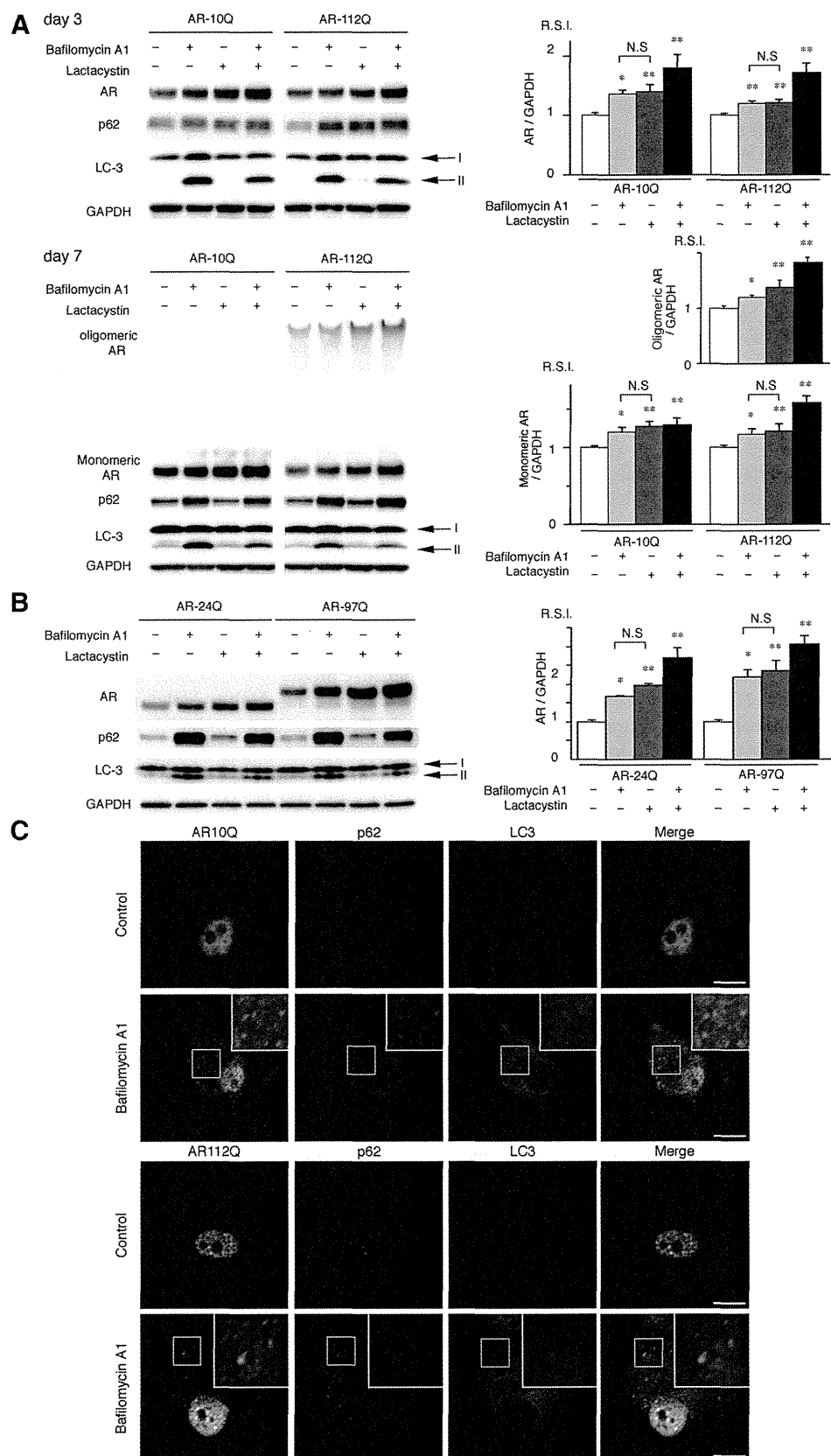
whether p62 can interact with the AR protein. Because wild-type p62 was difficult to use in immunoprecipitation assay experiments given its propensity for aggregation, we used p62 with a PB1 (Phox and Bem1p) domain mutation (Fig. 2B–F). The self-oligomerization of p62 has been shown to be severely attenuated by this mutation (Lamark et al., 2003; Ichimura et al., 2008). In immunoprecipitation experiments, AR-24Q and AR-97Q coimmunoprecipitated with both endogenous and transfected p62, which suggests that p62 could either directly or indirectly recognize the AR (Fig. 2A–G). To determine the region of p62 that is required for the interaction with AR, we performed immunoprecipitation assay experiments using a series of p62 deletion mutants. The functional domains and exons of the corresponding mouse p62 gene were preserved in each construct (Fig. 2E). Deletion mutants of p62 (M6 and M7) failed to interact with the AR, whereas other mutants (M0–M5) interacted with the AR, which suggests that amino acid sequences from exon 4 (amino acids 180–225) of p62 are essential for its interaction with the AR (Fig. 2F). This AR–p62 interaction did not change when ubiquitin binding was disrupted using the M406V mutation in the p62 expression vector (Fig. 2G) (Falchetti et al., 2004). These results indicate that p62 can either directly or indirectly recognize the AR without ubiquitination and that the AR is degraded via autophagy.

### Depletion of p62 promotes the accumulation of AR in a cell culture model

To determine whether depletion of p62 influences the turnover of AR, we treated the inducible PC12 cells that expressed AR-10Q and AR-112Q with either control siRNA or p62 siRNA. Immunoblot analysis revealed the accumulation of both monomeric wild-type (AR-10Q) and mutant (AR-112Q) AR after DHT treatment for 3 and 7 d and the accumulation of a high-molecular-weight complex of the mutant AR in the AR-112Q cells after DHT treatment for 7 d in the PC12 cells that were depleted of p62 ( $p < 0.01$ ), which suggests that both wild-type and mutant ARs were degraded via p62-dependent autophagic degradation (Fig. 3A). Similar accumulations of AR-24Q, AR-97Q, and p62 were observed when we transiently transfected wild-type (AR-24Q) or mutant (AR-97Q) AR into Neuro2A cells and treated the cells with p62 siRNA (Fig. 3B). The turnover of wild-type (AR-10Q) and mutant (AR-112Q) ARs was then assessed using a pulse-chase labeling assay in PC12 cells to determine whether the enhanced degradation of AR was attributable to protein degradation or to a change in RNA expression. Wild-type and mutant ARs were degraded almost equally in the absence of p62 siRNA, as reported previously (Bailey et al., 2002; Lieberman et al., 2002). In the absence of p62, wild-type and mutant ARs exhibited markedly diminished degradation (Fig. 3C,D), whereas the mRNA levels for both AR-10Q and AR-112Q were quite similar when treated with control or p62 siRNA constructs (Fig. 3E). Similarly, the mRNA levels for both AR-24Q and AR-97Q in Neuro2A cells were approximately equal when treated with mock or p62 siRNA constructs (Fig. 3F). These data indicate that deprivation of p62 influenced the autophagic degradation of both wild-type and mutant proteins without altering the mRNA levels, even in cells with NIs.

### Depletion of p62 impairs the phenotypes of male AR-97Q mice

The aforementioned results suggest that endogenous p62 plays an important role in the degradation of misfolded polyQ protein in cells. We hypothesized that, if p62 contributes to the cellular



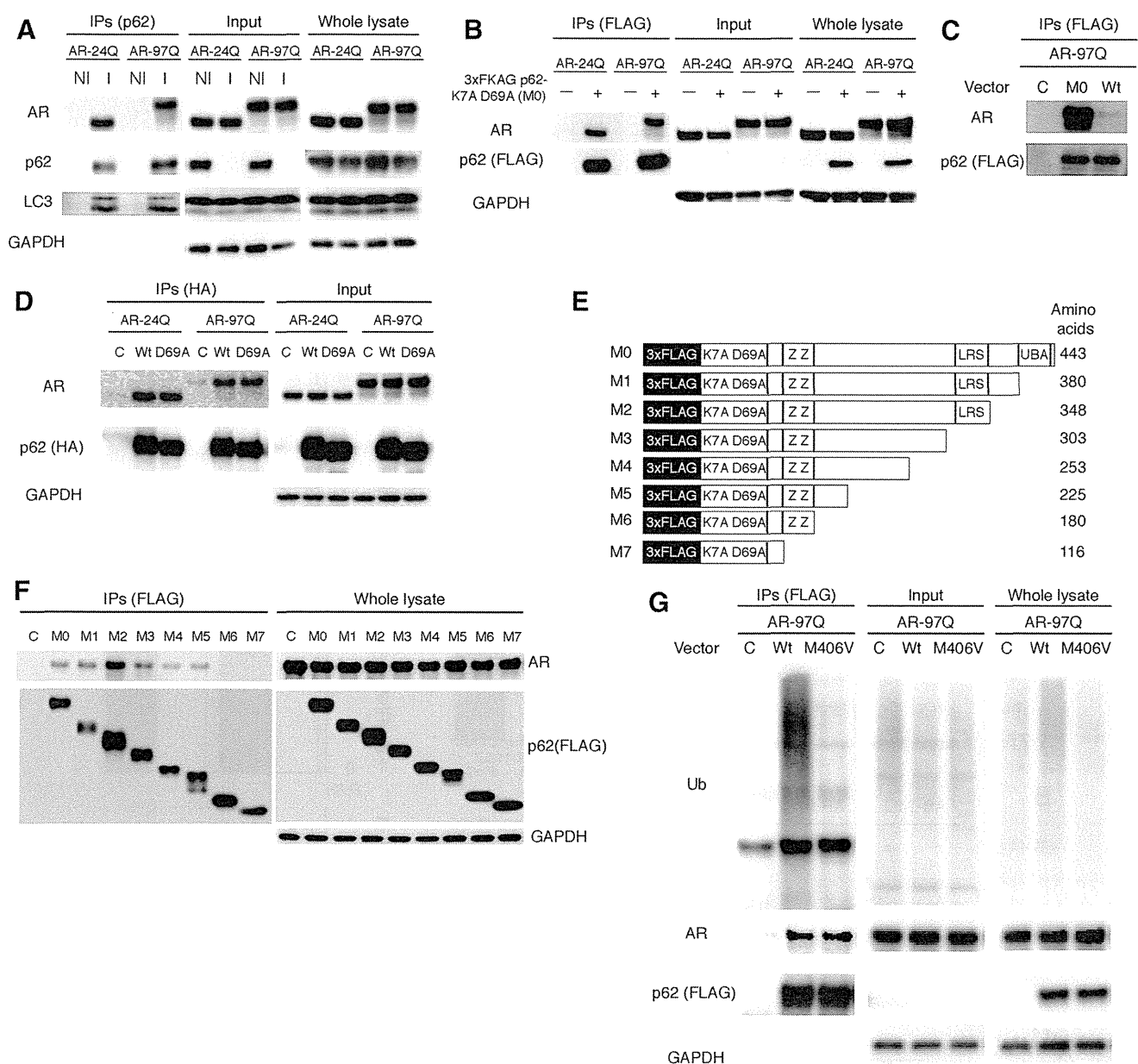


**Figure 2.** p62 interacts with AR. **A**, Neuro2A cells transfected with wild-type (24Q) and mutant (97Q) AR were treated with bafilomycin A1 (20 nM) for 16 h. Immunoprecipitation was then performed with non-immune rabbit IgG (NI) or an antibody for endogenous p62 (I). **B**, PB1 mutant p62 (M0) or wild-type p62 (Wt) and AR were cotransfected in Neuro2A cells, followed by immunoprecipitation with FLAG M2 agarose beads. Mutant p62 coprecipitated with AR, whereas the control did not show an interaction. **C**, PB1 mutant p62 (M0) and AR were cotransfected in Neuro2A cells. Immunoprecipitation was then performed using FLAG M2 agarose beads. **D**, p62 with an HA tag and ARs were cotransfected in Neuro2A cells. Immunoprecipitation was then performed using an HA antibody. **E**, A schematic representation of p62 deletion mutants fused with an N-terminal 3xFLAG generated by mutagenesis. **F**, AR-97Q and p62 mutants (M0–M7) were cotransfected, and immunoprecipitation was performed. **G**, Mutant p62 (M406V) or wild-type p62 (Wt) and AR-97Q were cotransfected in Neuro2A cells, followed by immunoprecipitation using FLAG M2 agarose beads. IPs, Immunoprecipitations; C, control; K7A D69A, Phox and Bem1p (PB1) domain with mutations for each amino acid; ZZ, ZZ-type zinc finger; LRS, LC3 recognition sequence; Ub, ubiquitin.

quality control of the mutant polyQ protein, then reducing the expression of p62 should exacerbate polyQ disease. To test this hypothesis *in vivo*, we crossed an SBMA transgenic mouse that overexpressed the full-length human AR with either 24Q or 97Q mice (AR-24Q or AR-97Q mice) with p62 knock-outs (−/−) (Komatsu et al., 2007). Because SBMA mice (AR-97Q mice) have a small body size, a shorter lifespan, progressive muscle atrophy and weakness, reduced cage activity, and a male preponderance similar to that of human SBMA patients (Katsuno et al., 2002), we used male transgenic mice in this study. The disease progression in the AR-97Q mice that had a homozygous depletion of p62

(AR-97Q/p62<sup>−/−</sup>) was significantly exacerbated compared with the disease progression in SBMA transgenic mice with normal p62 activity (AR-97Q/p62<sup>+/+</sup>) and in AR-97Q/p62<sup>+/−</sup> mice with a heterozygous depletion of p62. Immunohistochemical studies of the spinal anterior horn and muscle using the p62-specific antibody in AR-97Q/p62<sup>+/+</sup> and AR-97Q/p62<sup>−/−</sup> mice confirmed the absence of p62 staining in the nuclei and cytoplasm of knock-out animals (Fig. 4A–D). Western blotting analysis confirmed the decline of p62 expression in the spinal cord and muscle of p62<sup>+/−</sup> mice and p62<sup>−/−</sup> mice (Fig. 4E). Mice of all three genotypes appeared to be normal until 6–9 weeks of age.

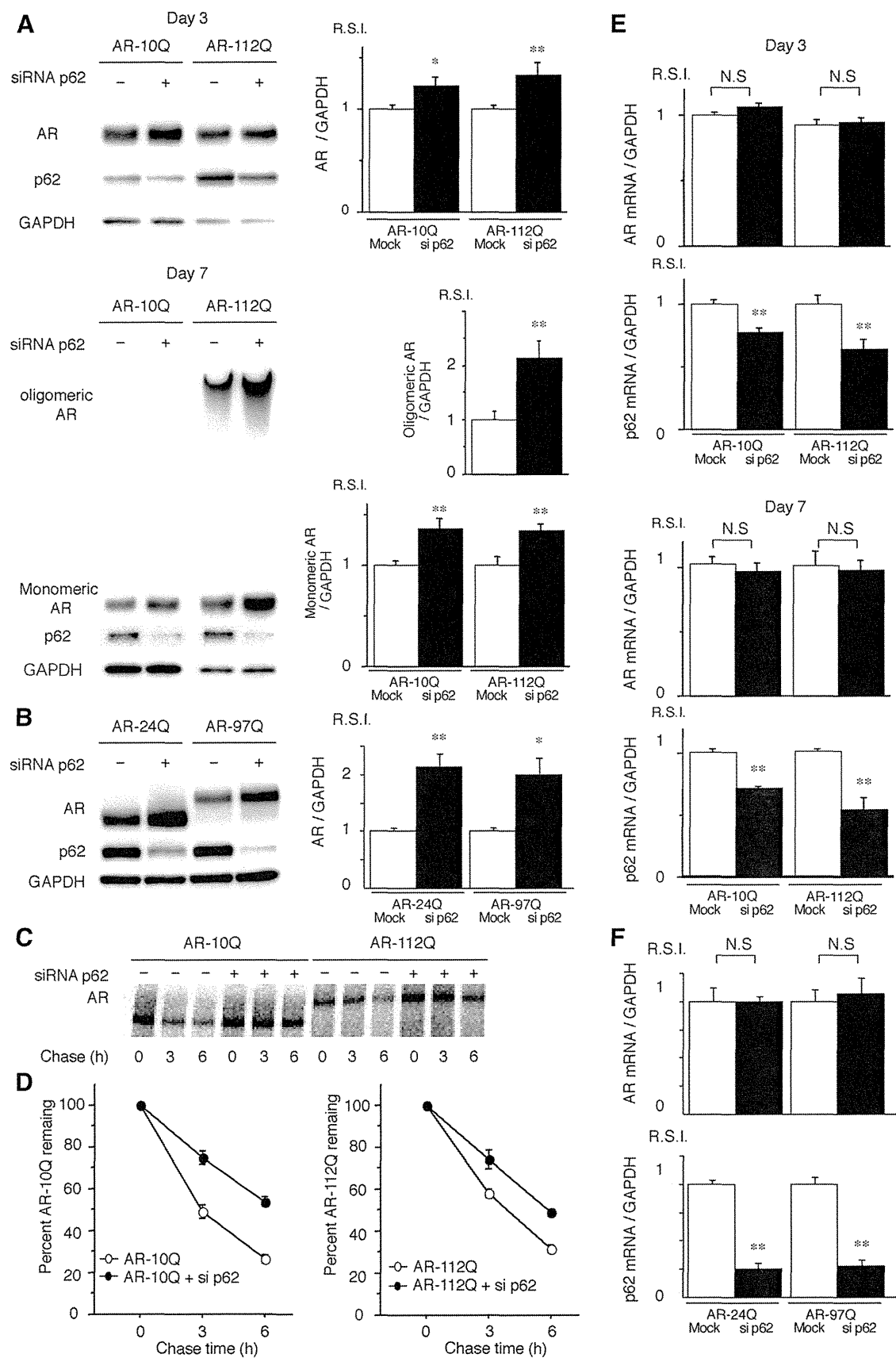


**Figure 3.** Depletion of p62 promotes the accumulation of AR. **A**, PC12 cells expressing wild-type (10Q) and mutant (112Q) AR were transfected with either control or p62 siRNA. The cells were treated with DHT for 3 or 7 d. **B**, Neuro2A cells transfected with wild-type (24Q) and mutant (97Q) AR were cotransfected with control or p62 siRNA. **C**, Pulse-chase analysis of two forms of AR in PC12 cells. Data from one representative experiment for wild-type and mutant AR. **D**, Pulse-chase assessment of half-life of the wild-type (left) and mutant AR (right). The percentages (*Figure legend continues.*)

However, by 10–15 weeks, the AR-97Q/p62<sup>-/-</sup> mice displayed prominent kyphosis, muscle weakness and atrophy, and a foot-dragging walk with foot inversion (Fig. 4F–K). After onset, the phenotype of the AR-97Q/p62<sup>-/-</sup> mice progressed rapidly to death over a 10–20 week period. By 20 weeks, only 10% of the AR-97Q/p62<sup>-/-</sup> mice remained alive, in contrast to ~40% of the AR-97Q/p62<sup>+/+</sup> mice (Fig. 4J). Furthermore, up to 25 weeks of age, none of the AR-24Q/p62<sup>-/-</sup> mice showed any neurological phenotypes (data not shown).

To further characterize the motor phenotype of these mice, we performed rotarod testing for 15-week-old AR-97Q/p62<sup>+/+</sup> and AR-97Q/p62<sup>-/-</sup> mice. AR-97Q/p62<sup>-/-</sup> mice exhibited significant motor impairment as assessed by the rotarod task when compared with AR-97Q/p62<sup>+/+</sup> mice ( $p < 0.05$ ; Fig. 4F). Locomotor cage activity for AR-97Q/p62<sup>-/-</sup> and AR-97Q/p62<sup>+/+</sup> mice was also significantly decreased when compared with that of the AR-97Q/p62<sup>+/+</sup> mice ( $p < 0.01$  and  $0.05$ , respectively; Fig. 4G). AR-97Q/p62<sup>-/-</sup> mice consistently performed more poorly than the other genotypes in tasks for testing grip strength ( $p < 0.01$ ; Fig. 4H). In addition, none of the genotypes were distinguishable in terms of body weight at birth. However, AR-97Q/p62<sup>-/-</sup> mice lost weight significantly earlier and more profoundly when compared with AR-97Q/p62<sup>+/+</sup> mice ( $p < 0.01$ ; Fig. 4I). Depletion of p62 also significantly decreased the survival rate of SBMA mice when compared with AR-97Q/p62<sup>+/+</sup> mice (AR-97Q/p62<sup>+/+</sup> vs AR-97Q/p62<sup>-/-</sup>,  $p = 0.247$  vs AR-97Q/p62<sup>-/-</sup>,  $p = 0.007$ ; Fig. 4J). Moreover, AR-97Q/p62<sup>-/-</sup> mice exhibited early onset of motor weakness, with dragging legs and shorter steps when compared with AR-97Q/p62<sup>+/+</sup> mice (Fig. 4K). Although the AR-97Q/p62<sup>-/-</sup> and AR-97Q/p62<sup>+/+</sup> mice both showed phenotypic expression, the AR-97Q/p62<sup>+/+</sup> mice had better performance than the AR-97Q/p62<sup>-/-</sup> mice for most of these parameters, which suggests that the affected motor phenotype depended on the expression level of p62 rather than the genetic background.

### Depletion of p62 induces the accumulation of ARs in an SBMA mouse model

We immunohistochemically examined mouse tissue samples for mutant ARs using the 1C2 antibody, which specifically recognizes expanded polyQs, and we noted a marked increase in DNS in the spinal cord (Fig. 5A–C) and muscles (Fig. 5D–F) in AR-97Q/p62<sup>-/-</sup> mice at 13 weeks when compared with the AR-97Q/p62<sup>+/+</sup> and AR-97Q/p62<sup>+/+</sup> mice. Quantitative assessments showed significantly more 1C2-positive cells in the spinal cord (Fig. 5G) and muscles (Fig. 5H) of AR-97Q/p62<sup>-/-</sup> mice when compared with AR-97Q/p62<sup>+/+</sup> mice. Because wild-type and mutant ARs similarly accumulate in the absence of p62 *in vitro*, we also examined the expression of ARs in SBMA mice. Western blotting analysis of lysates from the spinal cord and muscle of AR-97Q mice revealed a high-molecular-weight mutant AR protein complex that was retained in the stacking gel as smear-shaped bands in addition to a band that could represent the monomeric mutant AR. Moreover, only the band for the wild-type monomeric AR was visible in the tissue from the AR-24Q mice (Fig. 5I,J). Depletion of p62 significantly increased the

amount of the high-molecular-weight complex, the monomeric form of the mutant AR in the spinal cord and muscle of AR-97Q mice, and the amount of wild-type monomeric AR in AR-24Q mice (Fig. 5I,J). These observations indicate that p62 affects p62-dependent degradation of wild-type and mutant AR proteins via autophagy. Anti-GFAP antibody staining showed an apparent increase in reactive astrogliosis in AR-97Q/p62<sup>-/-</sup> mice when compared with AR-97Q/p62<sup>+/+</sup> mice in the spinal anterior horn (Fig. 5K,L). Western blotting analyses using an antibody against GFAP revealed that depletion of p62 upregulated GFAP, which indicates that the depletion of p62 exacerbated the neurodegenerative changes (Fig. 5M). Muscle histology and weight measurement also revealed significant exacerbation of muscle atrophy in AR-97Q/p62<sup>-/-</sup> mice compared with AR-97Q/p62<sup>+/+</sup> mice (Fig. 5N–P). Depletion of p62 did not influence the expression of total ubiquitinated proteins in the spinal cord and muscle of AR-24Q and AR-97Q mice, as determined by ubiquitin staining of Western blots (Fig. 5Q) and histology (data not shown).

### p62 overexpression ameliorates phenotypes in male AR-97Q mice

To test whether increased expression of p62 provides protective effects in AR-97Q mice, we generated transgenic mice that overexpressed full-length human p62 with a C-terminal HA tag under the control of a cytomegalovirus enhancer and a chicken  $\beta$ -actin promoter (Fig. 6A). The promoter used for this transgenic mouse was the same as that used in the SBMA model mice. Among 10 available mouse lines, we established four that expressed p62 in the spinal cord and skeletal muscle, and we examined the effects of the overexpressed p62 on mouse phenotypes. Western blotting analysis revealed that p62 expression in the spinal cords of p62<sup>(tg/+)</sup> mice was fourfold higher than the expression of endogenous p62 in wild-type mice. In muscle, p62 expression was 12-fold higher in p62<sup>(tg/+)</sup> mice compared with wild-type mice (Fig. 6B). Immunohistochemical studies performed on p62<sup>(tg/+)</sup> mouse tissue using an anti-HA tag antibody confirmed that spinal anterior horn neurons and muscle cells expressed p62. Moreover, p62 protein was distributed in the cytoplasm and nuclei of the spinal anterior horn neurons, glial cells, and muscles (Fig. 6C,D). Up to 35 weeks of age, none of the hemizygous transgenic mice that overexpressed p62 presented any neurological phenotypes, as assessed by the rotarod task, cage activity, grip strength, and body weight (data not shown). Histological examination at 35 weeks did not reveal any detectable effects on neuronal cell morphology, neuronal cell number, or muscle structure (data not shown). These studies indicate that overexpression of human p62 alone does not impair neuronal development or motor function.

We crossed the AR-24Q and AR-97Q mice with mice that overexpress human p62 (p62 1–1 line) to generate hemizygous AR-24Q/p62<sup>(tg/+)</sup> and AR-97Q/p62<sup>(tg/+)</sup> mice and AR-24Q/p62<sup>(+/+)</sup> and AR-97Q/p62<sup>(+/+)</sup> mice for use as controls. The AR-97Q mice that overexpressed p62 (AR-97Q/p62<sup>(tg/+)</sup>) demonstrated amelioration of the disease course after 18 weeks of age (Fig. 6E–I). In addition, AR-97Q/p62<sup>(tg/+)</sup> mice showed improvements in their motor impairment, as assessed by the rotarod task at 25 weeks ( $p < 0.05$ ; Fig. 6E). Locomotor cage activity of the AR-97Q/p62<sup>(tg/+)</sup> mice was also significantly increased at 25 weeks when compared with that of the AR-97Q/p62<sup>(+/+)</sup> mice ( $p < 0.05$ ; Fig. 6F). Furthermore, grip strength was stronger in the AR-97Q/p62<sup>(tg/+)</sup> mice than in the control mice ( $p < 0.05$ ; Fig. 6G), and AR-97Q/p62<sup>(+/+)</sup> mice lost weight significantly earlier and more profoundly than the AR-97Q/

(Figure legend continued.) of wild-type (10Q) and mutant (112Q) remaining in the presence (●) and absence (○) of p62 siRNA are indicated. **E**, Real-time RT-PCR for wild-type (10Q) and mutant (112Q) AR mRNA normalized to GAPDH levels in PC12 cells. **F**, Real-time RT-PCR for wild-type (24Q) and mutant (97Q) AR mRNA normalized to GAPDH levels in Neuro2A cells. These experiments were repeated in five sets of cells, and equivalent results were obtained. All of the values are expressed as the means  $\pm$  SEM ( $n = 5$ ). \* $p < 0.05$ ; \*\* $p < 0.01$ .

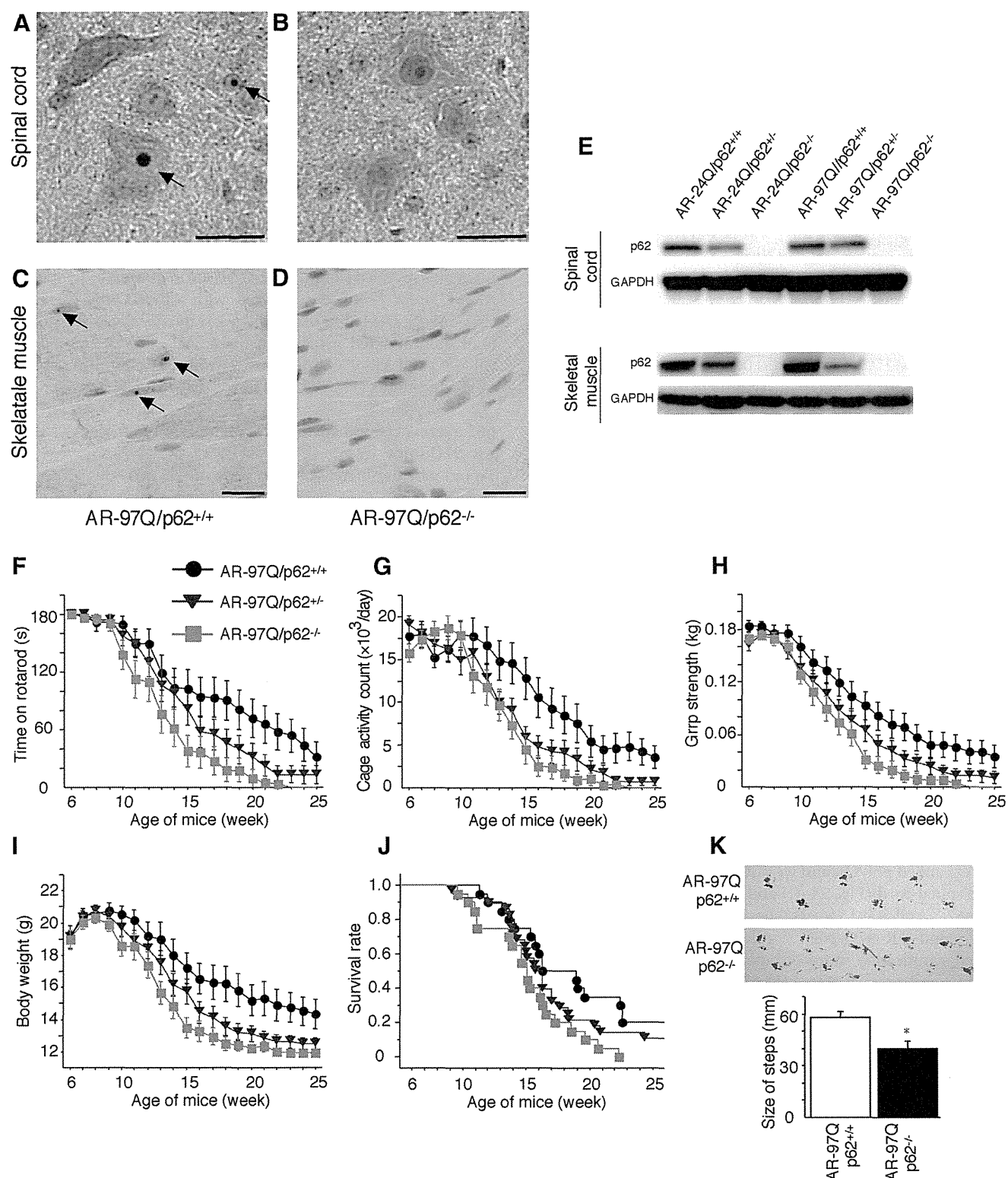


**Figure 4.** Depletion of p62 impairs behavioral and visible phenotypes in male AR-97Q mice. **A–D**, p62 immunohistochemistry in the spinal anterior horn (**A**, **B**) and skeletal muscle (**C**, **D**) of 25-week-old AR-97Q/p62<sup>+/+</sup> (**A**, **C**) and 13-week-old AR-97Q/p62<sup>-/-</sup> (**B**, **D**) mice counterstained with Mayer's hematoxylin. p62 immunoreactivity was localized to the nuclei and cytoplasm, with NIs (arrow) in the anterior horn cells and skeletal muscle. Scale bars, 20  $\mu$ m. **E**, Western blotting analysis of p62 expression in the total spinal cord and muscle protein lysates from the indicated mice immunolabeled with antibodies against p62. **F–J**, Rotarod task (**F**), cage activity (**G**), grip strength (**H**), body weight (**I**), and survival rate (**J**) of the AR-97Q/p62<sup>+/+</sup> (●;  $n = 20$ ), AR-97Q/p62<sup>+/-</sup> (▼;  $n = 28$ ), and AR-97Q/p62<sup>-/-</sup> (■;  $n = 20$ ) mice. Although none of the parameters tested at 15 weeks revealed significant differences between AR-97Q/p62<sup>+/-</sup> and AR-97Q/p62<sup>+/+</sup> mice, the AR-97Q/p62<sup>+/-</sup> mice performed more poorly than the AR-97Q/p62<sup>+/+</sup> mice in all of the parameters. **K**, Footprints of representative 13-week-old AR-97Q/p62<sup>+/+</sup> and AR-97Q/p62<sup>-/-</sup> mice. The front paws are indicated in blue, and the hindpaws are indicated in red. Values are expressed as the means  $\pm$  SEM. \* $p < 0.05$ .



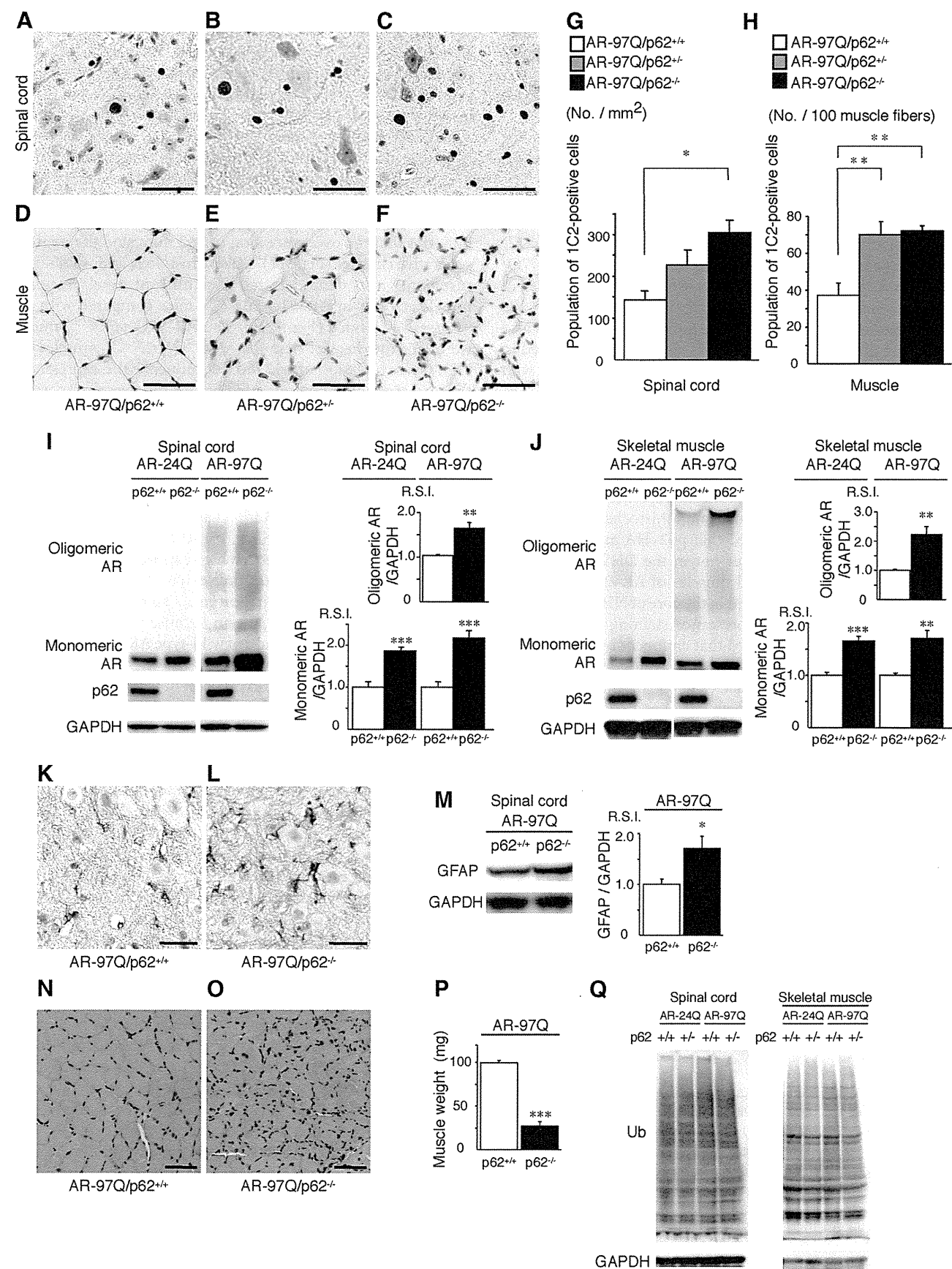


**Figure 5.** Depletion of p62 induces the accumulation of AR in an SBMA mouse model. **A–F**, PolyQ immunohistochemistry (1C2) in the spinal anterior horn (**A–C**) and muscle (**D–F**) of 13-week-old AR-97Q/p62<sup>+/+</sup>, AR-97Q/p62<sup>+/-</sup>, and AR-97Q/p62<sup>-/-</sup> mice. Scale bars, 50  $\mu$ m. **G, H**, Quantitative assessment of 1C2 staining in the spinal ventral horn (**G**) and muscle (**H**). (Figure legend continues.)

$p62^{tg/+}$  mice ( $p < 0.05$ ; Fig. 6H). An increase in p62 also significantly increased the survival rate of AR-97Q/ $p62^{tg/+}$  mice compared with AR-97Q/ $p62^{+/+}$  mice ( $p = 0.008$ ; Fig. 6I). Although the AR-97Q/ $p62^{tg/+}$  mice took relatively shorter steps than the wild-type mice, they walked with significantly longer steps than the AR-97Q/ $p62^{+/+}$  mice ( $p < 0.01$ ; Fig. 6J).

### p62 overexpression promotes NI body formation and reduces DNS of mutant AR in an SBMA mouse model

We performed immunohistochemical staining for mutant AR using the 1C2 antibody in the spinal cord and skeletal muscle of 25-week-old mice. Intriguingly, numerous NIs of the mutant AR were observed in AR-97Q/ $p62^{tg/+}$  mice but not in AR-97Q/ $p62^{+/+}$  mice (Fig. 7A). The intensity of the DNS was reduced in cells with NIs (Fig. 7A, arrow) compared with cells without NIs (Fig. 7A, arrowhead). The ratio of the number of cells with NIs to the number of total 1C2-positive cells significantly increased in AR-97Q/ $p62^{tg/+}$  mice (Fig. 7B), and the number of cells with DNS was significantly decreased in AR-97Q/ $p62^{tg/+}$  mice (Fig. 7C). The R.S.I. of the DNS was significantly reduced in cells with NIs compared with those without NIs in the spinal anterior horn and skeletal muscle (Fig. 7D). We evaluated the colocalization of overexpressed human p62 and mutant AR in AR-97Q/ $p62^{tg/+}$  mice. Intriguingly, double-immunofluorescence staining with anti-HA and 1C2 antibodies and immunohistochemistry with an anti-HA antibody demonstrated that p62-HA and mutant AR colocalized in all of the NIs but not in the DNS in the spinal anterior horn cells and skeletal muscles of AR-97Q mice (Fig. 7E–H). In addition, p62 localized in the core of NIs of mutant AR (Fig. 7I). Double-immunofluorescence staining with anti-p62 and 1C2 antibodies also revealed that endogenous p62 and mutant AR colocalized in the NIs in the spinal anterior horn cells and skeletal muscles of AR-97Q mice (Fig. 8A,B) and in the spinal anterior horn neurons of human SBMA patients (Fig. 8C,D), which suggests that endogenous p62 coexists with mutant AR and can exert a cell-protective function in both AR-97Q mice and SBMA patients. There were no NIs in the spinal cord and skeletal muscle of the AR-24Q/ $p62^{tg/+}$  mice (data not shown).

### p62 overexpression reduces the monomeric and oligomeric protein expression of mutant AR in an SBMA mouse model

Overexpression of p62 significantly decreased the amount of the high-molecular-weight mutant AR protein complex and the monomeric form of the mutant AR (AR-97Q) in the spinal cord and skeletal muscle of AR-97Q mice, whereas it did not decrease the expression of wild-type monomeric AR (AR-24Q) (Fig. 9A,B). To address whether nuclear ARs shift from a more soluble oligomer to a less soluble and aggregated state in AR-97Q/ $p62^{tg/+}$  mice, we lysed the pellet in 8 M urea solution and performed

Western blotting. Overexpression of p62 significantly increased AR protein in the pellet of the spinal cord and skeletal muscle of AR-97Q/ $p62^{tg/+}$  mice, suggesting that increasing p62 shifts from soluble oligomeric AR to insoluble AR (Fig. 9C,D). The respective levels of wild-type and mutant AR mRNA were similar in AR-24Q and AR-97Q mice overexpressing p62 (Fig. 9E). Anti-GFAP staining showed an apparent decrease in reactive astrogliosis in AR-97Q/ $p62^{tg/+}$  mice when compared with AR-97Q/ $p62^{+/+}$  mice in the spinal anterior horn (Fig. 9F,G). Western blotting analyses with an antibody against GFAP revealed that overexpression of p62 downregulated GFAP, which indicates that the overexpression of p62 mitigated the neurodegenerative changes (Fig. 9H). Muscle histology and weight measurements also demonstrated a significant amelioration of muscle atrophy in AR-97Q/ $p62^{tg/+}$  mice compared with AR-97Q/ $p62^{+/+}$  mice (Fig. 9I,J). The AR-97Q/ $p62^{tg/+}$  muscles were 2.2 times heavier than the AR-97Q/ $p62^{+/+}$  muscles (Fig. 9K). Overexpression of p62 did not influence the expression of the total amount of ubiquitinated proteins in the spinal cord and muscle of AR-24Q and AR-97Q mice, as determined by Western blots (Fig. 9L), whereas more ubiquitin-positive NIs were identified in the AR-97Q/ $p62^{tg/+}$  mice than in the AR-97Q/ $p62^{+/+}$  mice (Fig. 9M,N). The expression of the autophagic marker LC3 (Mizushima et al., 2010) was slightly elevated in the spinal cord and muscle of AR-24Q/ $p62^{tg/+}$  and AR-97Q/ $p62^{tg/+}$  mice compared with AR-24Q/ $p62^{+/+}$  and AR-97Q/ $p62^{+/+}$  mice (Fig. 10A,B), which suggests that high expression of p62 induced autophagosome formation to some extent. However, the induction of autophagosome formation could be insufficient to affect the degradation of the AR protein because p62 overexpression did not decrease the expression of wild-type AR in the spinal cord and skeletal muscle of AR-24Q mice (Fig. 9A,B). Overexpression of p62 did not influence the expression of wild-type and mutant AR in two SBMA cellular models (Fig. 11A,B). In this culture system, we detected a band that represented a monomeric mutant AR in the separating gel. However, it was difficult to detect the high-molecular-weight mutant AR protein complex and NIs. Thus, this cell culture model is more appropriate for estimating changes in monomeric mutant AR expression. These observations suggest that an increase in p62 promotes the downregulation of soluble-toxic mutant AR species via harmless inclusion body formation rather than by autophagic degradation and exerts therapeutic effects in AR-97Q mice. Our results were consistent with those of a previous study that showed that NI formation exhibits protective effects in a cellular model of Huntington's disease (Arrasate et al., 2004).

### Discussion

The protein p62 is a ubiquitously expressed cellular protein, and it has been shown recently to be a selective substrate for autophagy (Bjørkøy et al., 2005; Pankiv et al., 2007; Ichimura et al., 2008). This protein is localized at the autophagosome formation site (Itakura and Mizushima, 2011) and directly interacts with LC3, which is an autophagosome-localizing protein (Pankiv et al., 2007; Ichimura et al., 2008). Subsequently, p62 incorporates into the autophagosome and is then degraded (Pankiv et al., 2007; Ichimura et al., 2008). Thus, impaired autophagy is accompanied by the accumulation of p62, followed by the formation of p62- and ubiquitin-positive aggregates because of the nature of self-oligomerization and ubiquitin binding by p62 (Mizushima and Komatsu, 2011). In contrast, inclusion bodies that are positive for both ubiquitin and p62 have been identified in various neurodegenerative disorders (Kuusisto et al., 2001,

(Figure legend continued.) Bars represent the density of 1C2-positive cells in AR-97Q/ $p62^{+/+}$ , AR-97Q/ $p62^{+/-}$ , and AR-97Q/ $p62^{-/-}$  mice. The results are expressed as the means  $\pm$  SEM ( $n = 6$ ). **I, J**, Western blotting analysis of the total tissue homogenates from the spinal cord (**I**) and muscle (**J**) of AR-24Q and AR-97Q mice (13 weeks of age,  $n = 6$ ), probed with anti-AR. Values are expressed as the means  $\pm$  SEM ( $n = 6$ ). **K, L**, Immunohistochemical staining with anti-GFAP antibody in the spinal anterior horn. Scale bars, 30  $\mu$ m. **M**, Western blotting analysis of the total tissue homogenates from the spinal cord of AR-97Q mice (13 weeks of age,  $n = 6$ ) probed with anti-GFAP. **N, O**, Hematoxylin and eosin staining of the muscles. **P**, The gastrocnemius muscles from AR-97Q/ $p62^{+/+}$  and AR-97Q/ $p62^{-/-}$  mice were dissected and weighed. **Q**, Western blotting analysis of the total tissue homogenates from the spinal cord and muscle of AR-24Q and AR-97Q mice (13 weeks of age) probed with anti-ubiquitin (Ub). Scale bars, 50  $\mu$ m. \* $p < 0.05$ ; \*\* $p < 0.01$ ; \*\*\* $p < 0.001$ .



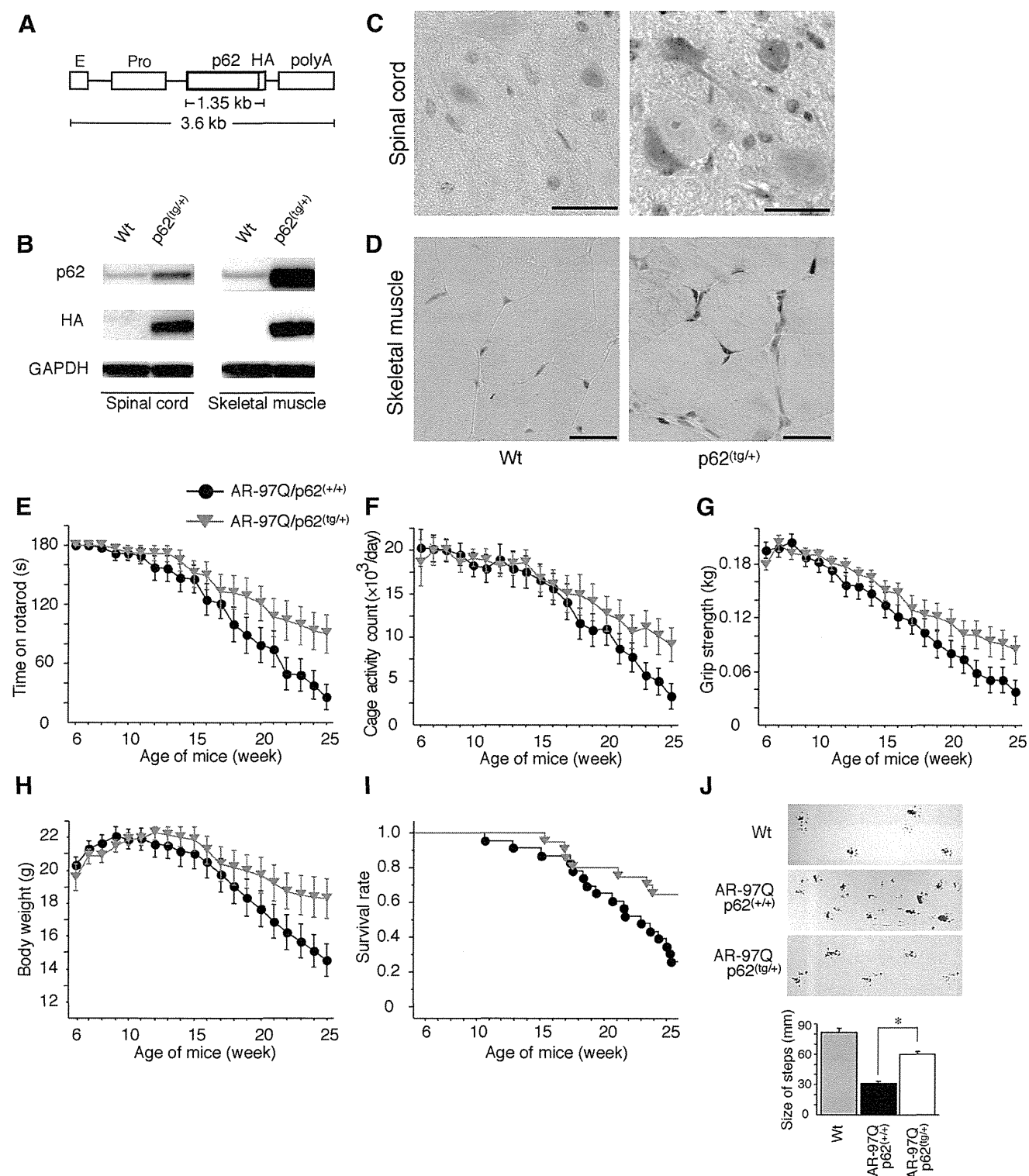


**Figure 6.** p62 overexpression ameliorates behavioral and visible phenotypes in male AR-97Q mice. **A**, A schematic view of the transgene construct. The microinjected fragment was composed of a cytomegalovirus enhancer (E), a chicken  $\beta$ -actin promoter (Pro), full-length human p62 with an HA tag, and a rabbit  $\beta$ -globin polyadenylation signal sequence (polyA). **B**, Western blotting analysis of total spinal cord and muscle protein lysates from wild-type (Wt) and  $p62^{tg/+}$  mice immunolabeled with antibodies against p62 and HA. **C**, **D**, HA immunohistochemistry in the spinal anterior horn (C) and skeletal muscle (D) of 13-week-old wild-type (Wt) and  $p62^{tg/+}$  mice counterstained with Mayer's hematoxylin. p62 immunoreactivity localized to the nuclei and cytoplasm of anterior horn cells (C) and skeletal muscle (D). HA staining was absent in the wild-type mice. Scale bars, 50  $\mu$ m. **E–I**, Rotarod task (E), cage activity (F), grip strength (G), body weight (H), and survival rate (I) of AR-97Q/ $p62^{+/+}$  (●;  $n = 25$ ) and AR-97Q/ $p62^{tg/+}$  (▼;  $n = 21$ ) mice. **J**, Footprints of representative 25-week-old AR-97Q/ $p62^{+/+}$  and AR-97Q/ $p62^{tg/+}$  mice. The front paws are indicated in blue, and the hindpaws are indicated in red. Values are expressed as the means  $\pm$  SEM. \* $p < 0.01$ .

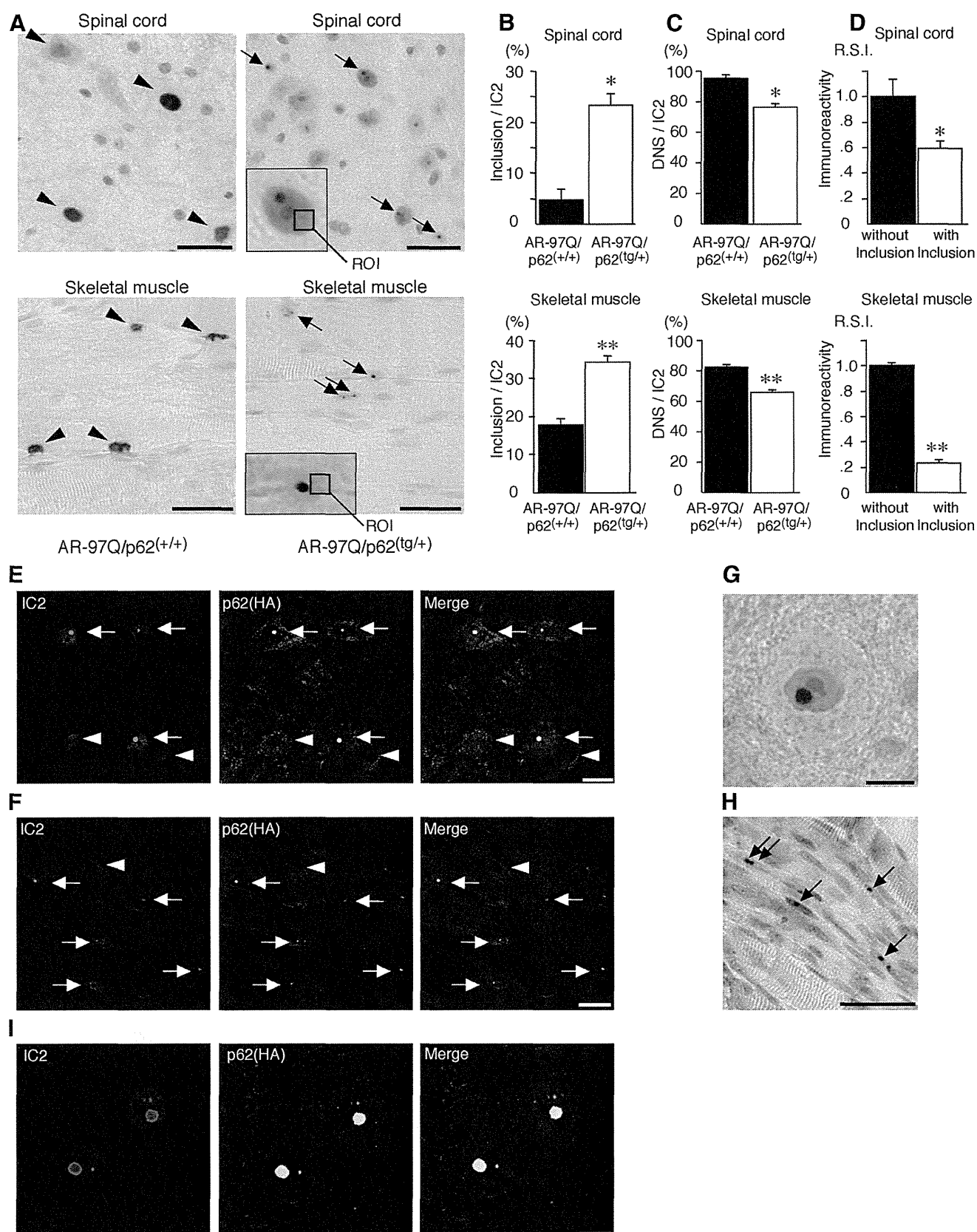


**Figure 7.** p62 promotes inclusion body formation of ARs in male AR-97Q mice. **A**, Immunohistochemical staining with 1C2 antibody revealed DNS (arrowhead) in AR-97Q/p62<sup>(+/+)</sup> mice and many NIs (arrow) in the AR-97Q/p62<sup>(tg/+)</sup> mice in the spinal anterior horn and skeletal muscle at 25 weeks of age. The region of interest for the DNS is defined as the ROI (inset; open square). Scale bars, 30  $\mu$ m. **B**, The ratio of the number of cells with NIs to the total number of IC2-positive cells. **C**, The ratio of the number of cells with DNS to the total number of IC2-positive cells. **D**, The R.S.I. of the DNS was significantly reduced in cells with NIs compared with those without NIs in spinal anterior horn neurons and skeletal muscle. **E**, **F**, Double-immunofluorescence staining with 1C2 (red) and anti-HA (green) antibodies in the spinal anterior horn (**E**) and skeletal muscle (**F**) of AR-97Q/p62<sup>(tg/+)</sup> mice revealed the complete colocalization of HA-tagged p62 and (Figure legend continues.)

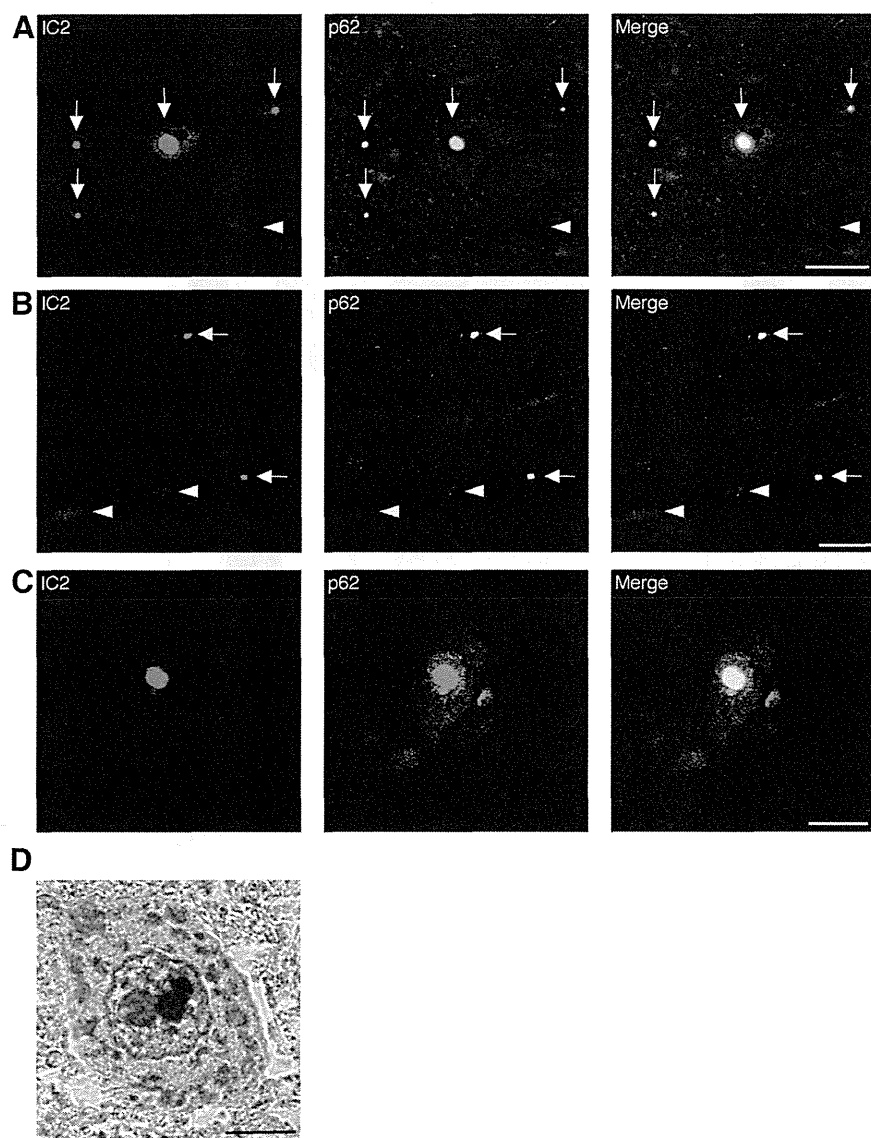


**Figure 8.** Colocalization of nuclear-localized p62 with mutant AR. **A–C**, IC2 (red) and anti-HA (green) double immunofluorescence in the spinal cord (**A**) and skeletal muscle (**B**) of 16-week-old AR-97Q mice and in the spinal anterior horn cells (**C**) of SBMA patients. Double-immunofluorescence staining revealed p62 and mutant AR colocalization in NIs (shown in yellow, arrow), but no colocalization was observed in the DNS (arrowhead) in AR-97Q mice and SBMA patients. Scale bars, 20  $\mu$ m. **D**, Immunohistochemistry for the anti-p62 antibody in SBMA patients. p62 was localized in the NIs. Scale bar, 10  $\mu$ m.

2008), which suggests that p62 contributes to inclusion formation. Furthermore, p62-positive aggregates observed in hepatocytes and neurons of liver- and brain-specific Atg7-deficient mice are completely dispersed by the additional loss of p62 (Komatsu et al., 2007).

We generated an SBMA transgenic mouse model (AR-97Q) that displayed progressive muscular atrophy, weakness, and DNS and NIs of the mutant AR in neuronal and non-neuronal tissues (Katsuno et al., 2002). Because AR has a specific ligand (i.e.,

testosterone), the pathogenesis of SBMA is unique among the polyQ diseases (Katsuno et al., 2003). The success of androgen deprivation therapy in SBMA mouse models has been translated into clinical trials (Katsuno et al., 2010; Fernández-Rhodes et al., 2011). In addition, the elucidation of SBMA pathophysiology using animal models has led to the development of other therapeutics, including chaperone-related disease-modifying therapy (Waza et al., 2005; Tokui et al., 2009), posttranslational modification of the AR (Palazzolo et al., 2009; Montie et al., 2011), AR mRNA stability (Miyazaki et al., 2012), and modulation of the NH<sub>2</sub>-carboxyl-terminal interaction of the AR (Orr et al., 2010), which inhibit the pathogenic process of neuronal degeneration. Thus, there is increasing evidence that AR ligands, molecular chaperones-UPS, and autophagy play crucial roles in the pathogenesis of SBMA. Furthermore, mutant AR that bears an expanded polyQ repeat adopts an altered conformation that results in protein aggregation and inclusion formation; however, recent studies have suggested that soluble causative protein species that include protein aggregates, rather than protein inclusions, could be toxic; thus, they represent targets in the treatment of neurodegenerative disorders (Bauer and Nukina, 2009; Naiki and Nagai, 2009; Hands and Wyttenbach, 2010). In this study, we addressed the questions of whether depletion of p62 exacerbates neuropathological outcomes and whether overexpression of p62 can protect against mutant AR toxicity and exert therapeutic effects on the SBMA phenotype. Depletion of p62 significantly increased the accumulation of monomeric mutant AR and mutant AR protein complexes in AR-97Q mice via an impairment of autophagic degradation, whereas helpful inclusion body formation was promoted

in the spinal cord and muscle of the AR-97Q/p62 double transgenic mice.

In a neuronal cell culture model of SBMA, we demonstrated that decreasing levels of p62 inhibited the degradation of monomeric wild-type and mutant ARs even in cells with NIs, which suggests that p62 plays a pivotal role in AR protein turnover. Growing evidence indicates that p62, together with ubiquitinated proteins, is transported into autophagosomes, which suggests that p62 is a receptor for ubiquitinated proteins that is necessary for their degradation in lysosomes (Johansen and Lamark, 2011). As a receptor, p62 would also contribute to autophagic degradation of Parkin-mediated ubiquitinated mitochondria (Geisler et al., 2010). Furthermore, p62 is localized at the autophagosome formation site and directly interacts with LC3, which facilitates the delivery of its polyubiquitinated protein for lysosomal degradation (Ichimura et al., 2008). Subsequently, p62 is also incorporated into the autophagosome and is then degraded. In addition,

(Figure legend continued.) mutant AR in NIs (arrow), but no colocalization was observed in the DNS (arrowhead). Scale bars, 20  $\mu$ m. **G, H**, p62 immunohistochemistry in the spinal anterior horn neurons (**G**) and skeletal muscle (**H**) of AR-97Q/p62<sup>tg/+</sup> mice. Arrows indicate NIs. Scale bars: **G**, 30  $\mu$ m; **H**, 50  $\mu$ m. Values are expressed as the means  $\pm$  SEM ( $n = 6$ ). **I**, IC2 (red) and anti-HA (green) double immunofluorescence in the spinal cord of 25-week-old AR-97Q/p62<sup>tg/+</sup> mice. \* $p < 0.01$ ; \*\* $p < 0.001$ .

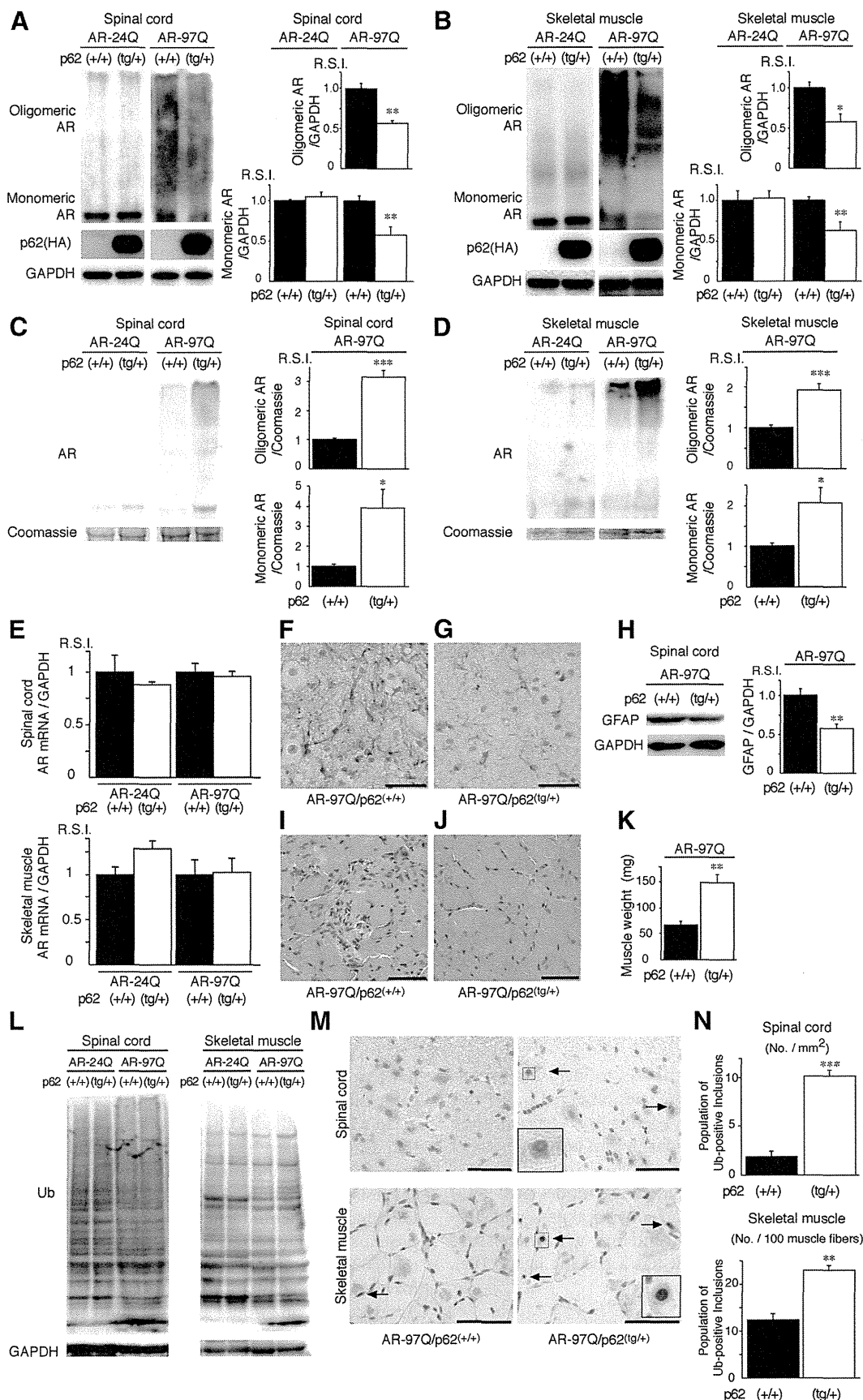


**Figure 9.** An increase in p62 reduces mutant AR expression. **A, B**, Western blotting analysis of total tissue homogenates from the spinal cord (**A**) and muscle (**B**) of AR-24Q and AR-97Q mice (25 weeks of age) probed with anti-AR. Values are expressed as the means ± SEM (n = 5). **C, D**, Western blotting analysis of the pellet lysed in 8 M urea solution from the spinal (*Figure legend continues.*)

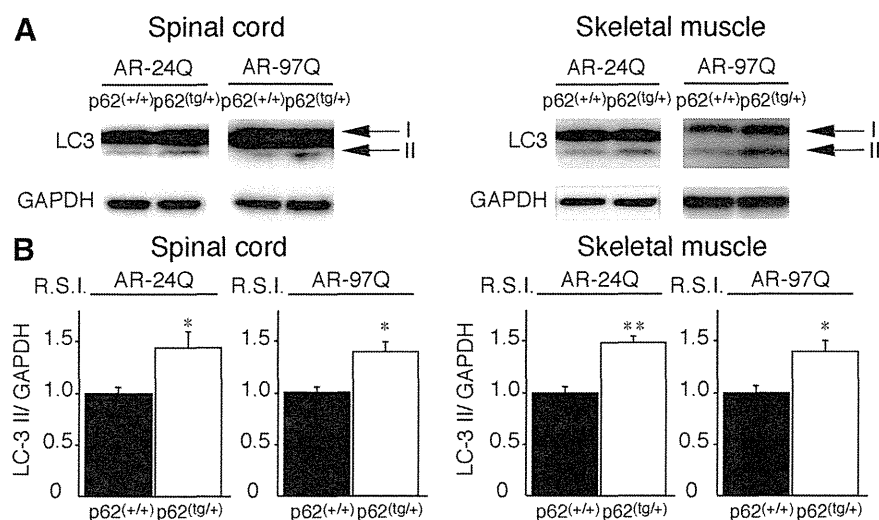


**Figure 10.** LC3-II expression in AR-97Q/p62<sup>tg/+</sup> mice. **A**, Western blotting analysis of total spinal cord protein lysates from the AR-97Q/p62<sup>tg/+</sup> and AR-97Q/p62<sup>tg/+</sup> mice immunolabeled with antibodies against LC3. **B**, Quantitative analysis for the amounts of LC3-II. LC3-II levels were slightly elevated in the AR-97Q/p62<sup>tg/+</sup> mice. This experiment was repeated in four sets of mice with equivalent results. All of the values are expressed as the means  $\pm$  SEM ( $n = 5$ ). \* $p < 0.05$ ; \*\* $p < 0.01$ .

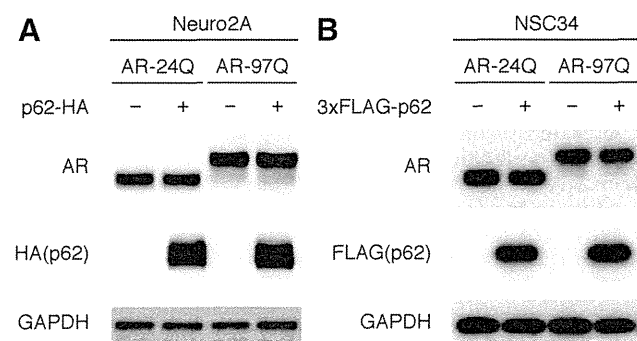


**Figure 11.** p62 overexpression does not affect AR expression. **A**, Full-length wild-type (24Q) or mutant (97Q) AR and HA-tagged p62 (pCAGGS-p62-HA) were cotransfected into Neuro2A cells for 48 h. **B**, Full-length wild-type (24Q) or mutant (97Q) AR and FLAG-tagged p62 (pIRES-puro3-3XFLAG-p62) were cotransfected into NSC34 cells for 48 h. All of the cells were cultured in DMEM/10% FCS at 37°C and with 5% CO<sub>2</sub>. Immunoblots revealed that the expression of AR was similar in the presence or absence of HA-p62 or FLAG-p62.

p62 has been shown to directly interact with mutant copper-zinc superoxide dismutase (SOD1) protein (Gal et al., 2007), which indicates that p62 directly or indirectly recognizes the mutant SOD1 protein and is degraded via autophagy. p62 also has the

capacity to sequester aggregate-prone proteins that might otherwise undergo proteasomal degradation (Korolchuk et al., 2009). In our study, both wild-type and mutant ARs colocalized with endogenous p62- and LC3-positive puncta (Fig. 1C). In addition, ARs were recognized directly by p62 (Fig. 2), which suggests that mutant AR is degraded in a p62-dependent autophagic pathway. Furthermore, our Western blotting analysis revealed that monomeric mutant AR and the high-molecular-weight form of mutant AR protein complexes retained in the stacking gel were upregulated in the spinal cord and muscle of AR-97Q transgenic/p62 knock-out mice, which suggests that degradation of mutant AR was inhibited by the deletion of p62.

In addition, the overexpression of p62 did not influence the expression of wild-type and mutant AR in a cellular model of SBMA or the expression of wild-type AR in a transgenic mouse model, which sug-

gests that p62 overexpression was not sufficient to promote the degradation of both wild-type and mutant AR (Figs. 9A,B, 11A,B). However, p62 overexpression enhanced the inclusion body formation of mutant ARs, which resulted in a reduction of expression in a transgenic mouse model (Figs. 7, 9), and this effect can occur independently of the degradation in lysosomes. More importantly, overexpressed p62 existed in all of the mutant AR NIs in the spinal cord and skeletal muscle of AR-97Q/p62 double transgenic mice. Furthermore, p62 also colocalized with mutant AR NIs that were present in the anterior horn cells of postmortem tissues obtained from SBMA patients. Inclusion bodies that were positive for both ubiquitin and p62 have been identified in various neurodegenerative diseases, which suggests that p62 is involved in the formation of disease-related inclusion bodies (Kuusisto et al., 2001, 2008; Labbadia et al., 2012). Intriguingly, the overexpressed p62 and mutant AR colocalized in all of the NIs but not in the DNS, and p62 was localized in the core of NIs of mutant AR (Fig. 7I). p62 can either directly or indirectly interact with the AR without its ubiquitination (Fig. 2G) and can also function with the misfolded AR, as indicated by the fact that we did not observe NI formation in the AR-24Q/p62<sup>tg/+</sup> mice. These results suggest that p62 is capable of self-oligomerization and could provide an opportunity for inclusion formation to generate the seeds of NIs.

However, the extent of diffuse nuclear accumulation of mutant AR in motor and sensory neurons of the spinal cord of autopsied SBMA patients was strongly correlated with the CAG repeat length but not with the number of NIs (Adachi et al., 2005). Accumulating evidence suggests that NIs are not harmful polyQ species (Arrasate et al., 2004) and instead that an oligomeric form of the mutant protein could be the major pathogenic species (Nagai et al., 2007; Sathasivam et al., 2010). Several studies have suggested that inclusion formation could be a cellular response against the toxicity of abnormal polyQ proteins (Arrasate et al., 2004; Bowman et al., 2005), whereas the nuclear localization or accumulation of abnormal proteins can be decisive in inducing neuronal cell dysfunction and degeneration in polyQ diseases, including SBMA (Klement et al., 1998; Saudou et al., 1998; Adachi et al., 2005). In view of the time course of SBMA,

(Figure legend continued.) cord (C) and muscle (D) of AR-24Q and AR-97Q mice (25 weeks of age) probed with anti-AR. Values are expressed as the means  $\pm$  SEM ( $n = 5$ ). **E**, Real-time RT-PCR of wild-type and mutant AR mRNA normalized to GAPDH levels. **F**, **G**, Immunohistochemical staining with anti-GFAP antibody in the spinal anterior horn. Scale bars, 30  $\mu$ m. **H**, Western blotting analysis of the total tissue homogenates from the spinal cord of AR-97Q mice (25 weeks of age,  $n = 5$ ) probed with anti-GFAP. **I**, **J**, Hematoxylin and eosin staining of the muscle. Scale bars, 50  $\mu$ m. **K**, The gastrocnemius muscles from AR-97Q/p62<sup>tg/+</sup> and AR-97Q/p62<sup>tg/+</sup> mice were dissected and weighed. **L**, Western blotting analysis of the total tissue homogenates from the spinal cord and muscle of AR-24Q and AR-97Q mice (25 weeks of age) probed with anti-ubiquitin (Ub). **M**, Ubiquitin immunohistochemistry revealed NIs (arrow) in the spinal anterior horn and muscle of 25-week-old AR-97Q/p62<sup>tg/+</sup> and AR-97Q/p62<sup>tg/+</sup> mice. The inset shows a magnified image in the square box. Scale bars, 50  $\mu$ m. **N**, Quantitative assessment of ubiquitin-positive NIs in the spinal ventral horn and muscle. Bars represent the density of ubiquitin-positive NIs in AR-97Q/p62<sup>tg/+</sup> and AR-97Q/p62<sup>tg/+</sup> mice. The results are expressed as the means  $\pm$  SEM ( $n = 6$ ). \* $p < 0.05$ ; \*\* $p < 0.01$ ; \*\*\* $p < 0.001$ .

diffuse nuclear accumulation of mutant proteins with an expanded polyQ tract might be an early event that occurs before NI formation, which is closely related to the manifestation of neuronal dysfunction (Watake et al., 2002; Yoo et al., 2003). The molecular pathogenetic process by which diffuse nuclear mutant AR accumulation induces neuronal dysfunction and death remains unclear; however, it is notable that overexpression of p62 can promote NI formation and the packaging of accumulated soluble and toxic nuclear mutant AR.

Accumulation of misfolded proteins is causally related to many age-related neurodegenerative diseases (Bates, 2006). Prompt removal and/or refolding could be required more in aged or damaged cells than in young healthy cells, in which protein quality control systems function appropriately. In SBMA patients, diffuse nuclear accumulation of mutant AR is frequent and extensive, and it occurs in a wide array of CNS nuclei and visceral organs. The precise mechanism used by the mutant protein must be determined in future studies; however, we have used cellular and mouse models of SBMA and demonstrated that p62 plays a beneficial role in autophagic degradation and NI formation of the mutant AR protein. These findings provide new insights into the cytoprotective functions of p62; thus, they could have important implications for the development of therapeutic strategies for the treatment of SBMA and other polyQ diseases.

## References

- Adachi H, Kume A, Li M, Nakagomi Y, Niwa H, Do J, Sang C, Kobayashi Y, Doyu M, Sobue G (2001) Transgenic mice with an expanded CAG repeat controlled by the human AR promoter show polyglutamine nuclear inclusions and neuronal dysfunction without neuronal cell death. *Hum Mol Genet* 10:1039–1048. CrossRef Medline
- Adachi H, Katsuno M, Minamiyama M, Waza M, Sang C, Nakagomi Y, Kobayashi Y, Tanaka F, Doyu M, Inukai A, Yoshida M, Hashizume Y, Sobue G (2005) Widespread nuclear and cytoplasmic accumulation of mutant androgen receptor in SBMA patients. *Brain* 128:659–670. CrossRef Medline
- Adachi H, Waza M, Katsuno M, Tanaka F, Doyu M, Sobue G (2007) Pathogenesis and molecular targeted therapy of spinal and bulbar muscular atrophy. *Neuropathol Appl Neurobiol* 33:135–151. CrossRef Medline
- Adachi H, Katsuno M, Waza M, Minamiyama M, Tanaka F, Sobue G (2009) Heat shock proteins in neurodegenerative diseases: pathogenic roles and therapeutic implications. *Int J Hyperthermia* 25:647–654. CrossRef Medline
- Al-Sarraj S, King A, Troakes C, Smith B, Maekawa S, Bodi I, Rogelj B, Al-Chalabi A, Hortobágyi T, Shaw CE (2011) p62 positive, TDP-43 negative, neuronal cytoplasmic and intranuclear inclusions in the cerebellum and hippocampus define the pathology of C9orf72-linked FTL and MND/ALS. *Acta Neuropathol* 122:691–702. CrossRef Medline
- Arrasate M, Mitra S, Schweitzer ES, Segal MR, Finkbeiner S (2004) Inclusion body formation reduces levels of mutant huntingtin and the risk of neuronal death. *Nature* 431:805–810. CrossRef Medline
- Bailey CK, Andriola IF, Kampinga HH, Merry DE (2002) Molecular chaperones enhance the degradation of expanded polyglutamine repeat androgen receptor in a cellular model of spinal and bulbar muscular atrophy. *Hum Mol Genet* 11:515–523. CrossRef Medline
- Bates GP (2006) BIOMEDICINE: one misfolded protein allows others to sneak by. *Science* 311:1385–1386. CrossRef Medline
- Bauer PO, Nukina N (2009) The pathogenic mechanisms of polyglutamine diseases and current therapeutic strategies. *J Neurochem* 110:1737–1765. CrossRef Medline
- Bjørkøy G, Lamark T, Brech A, Outzen H, Perander M, Overvatn A, Stenmark H, Johansen T (2005) p62/SQSTM1 forms protein aggregates degraded by autophagy and has a protective effect on huntingtin-induced cell death. *J Cell Biol* 171:603–614. CrossRef Medline
- Bowman AB, Yoo SY, Dantuma NP, Zoghbi HY (2005) Neuronal dysfunction in a polyglutamine disease model occurs in the absence of ubiquitin-proteasome system impairment and inversely correlates with the degree of nuclear inclusion formation. *Hum Mol Genet* 14:679–691. CrossRef Medline
- Buchberger A, Bukau B, Sommer T (2010) Protein quality control in the cytosol and the endoplasmic reticulum: brothers in arms. *Mol Cell* 40:238–252. CrossRef Medline
- Di Prospero NA, Fischbeck KH (2005) Therapeutics development for triplet repeat expansion diseases. *Nat Rev Genet* 6:756–765. CrossRef Medline
- Falchetti A, Di Stefano M, Marini F, Del Monte F, Mavilia C, Strigoli D, De Feo ML, Isaia G, Masi L, Amedei A, Cioppi F, Ghinoli V, Bonghi SM, Di Fede G, Sferazza C, Rini GB, Melchiorre D, Matucci-Cerinic M, Brandi ML (2004) Two novel mutations at exon 8 of the Sequestosome 1 (SQSTM1) gene in an Italian series of patients affected by Paget's disease of bone (PDB). *J Bone Miner Res* 19:1013–1017. CrossRef Medline
- Fernández-Rhodes LE, Kokkinis AD, White MJ, Watts CA, Auh S, Jeffries NO, Shrader JA, Lehky TJ, Li L, Ryder JE, Levy EW, Solomon BI, Harris-Love MO, La Pean A, Schindler AB, Chen C, Di Prospero NA, Fischbeck KH (2011) Efficacy and safety of dutasteride in patients with spinal and bulbar muscular atrophy: a randomised placebo-controlled trial. *Lancet Neurol* 10:140–147. CrossRef Medline
- Gal J, Ström AL, Kilty R, Zhang F, Zhu H (2007) p62 accumulates and enhances aggregate formation in model systems of familial amyotrophic lateral sclerosis. *J Biol Chem* 282:11068–11077. CrossRef Medline
- Geisler S, Holmström KM, Skujat D, Fiesel FC, Rothfuss OC, Kahle PJ, Springer W (2010) PINK1/Parkin-mediated mitophagy is dependent on VDAC1 and p62/SQSTM1. *Nat Cell Biol* 12:119–131. CrossRef Medline
- Hands SL, Wyttenbach A (2010) Neurotoxic protein oligomerisation associated with polyglutamine diseases. *Acta Neuropathol* 120:419–437. CrossRef Medline
- Ichimura Y, Komatsu M (2010) Selective degradation of p62 by autophagy. *Semin Immunopathol* 32:431–436. CrossRef Medline
- Ichimura Y, Kumanomidou T, Sou YS, Mizushima T, Ezaki J, Ueno T, Komimami E, Yamane T, Tanaka K, Komatsu M (2008) Structural basis for sorting mechanism of p62 in selective autophagy. *J Biol Chem* 283:22847–22857. CrossRef Medline
- Itakura E, Mizushima N (2011) p62 Targeting to the autophagosome formation site requires self-oligomerization but not LC3 binding. *J Cell Biol* 192:17–27. CrossRef Medline
- Johansen T, Lamark T (2011) Selective autophagy mediated by autophagic adapter proteins. *Autophagy* 7:279–296. CrossRef Medline
- Katsuno M, Banno H, Suzuki K, Takeuchi Y, Kawashima M, Yabe I, Sasaki H, Aoki M, Morita M, Nakano I, Kanai K, Ito S, Ishikawa K, Mizusawa H, Yamamoto T, Tsuji S, Hasegawa K, Shimohata T, Nishizawa M, Miyajima H, et al. (2010) Efficacy and safety of leuporelin in patients with spinal and bulbar muscular atrophy (JASMITT study): a multicentre, randomised, double-blind, placebo-controlled trial. *Lancet Neurol* 9:875–884. CrossRef Medline
- Katsuno M, Adachi H, Kume A, Li M, Nakagomi Y, Niwa H, Sang C, Kobayashi Y, Doyu M, Sobue G (2002) Testosterone reduction prevents phenotypic expression in a transgenic mouse model of spinal and bulbar muscular atrophy. *Neuron* 35:843–854. CrossRef Medline
- Katsuno M, Adachi H, Doyu M, Minamiyama M, Sang C, Kobayashi Y, Inukai A, Sobue G (2003) Leuporelin rescues polyglutamine-dependent phenotypes in a transgenic mouse model of spinal and bulbar muscular atrophy. *Nat Med* 9:768–773. CrossRef Medline
- King A, Maekawa S, Bodi I, Troakes C, Al-Sarraj S (2011) Ubiquitinated, p62 immunopositive cerebellar cortical neuronal inclusions are evident across the spectrum of TDP-43 proteinopathies but are only rarely additionally immunopositive for phosphorylation-dependent TDP-43. *Neuropathology* 31:239–249. CrossRef Medline
- Klement IA, Skinner PJ, Kaytor MD, Yi H, Hersch SM, Clark HB, Zoghbi HY, Orr HT (1998) Ataxin-1 nuclear localization and aggregation: role in polyglutamine-induced disease in SCA1 transgenic mice. *Cell* 95:41–53. CrossRef Medline
- Komatsu M, Waguri S, Koike M, Sou YS, Ueno T, Hara T, Mizushima N, Iwata J, Ezaki J, Murata S, Hamazaki J, Nishito Y, Iemura S, Natsume T, Yanagawa T, Uwayama J, Warabi E, Yoshida H, Ishii T, Kobayashi A, et al. (2007) Homeostatic levels of p62 control cytoplasmic inclusion body formation in autophagy-deficient mice. *Cell* 131:1149–1163. CrossRef Medline
- Korolchuk VI, Mansilla A, Menzies FM, Rubinsztein DC (2009) Autophagy inhibition compromises degradation of ubiquitin-proteasome pathway substrates. *Mol Cell* 33:517–527. CrossRef Medline
- Kuusisto E, Salminen A, Alafuzoff I (2001) Ubiquitin-binding protein p62 is



- present in neuronal and glial inclusions in human tauopathies and synucleinopathies. *Neuroreport* 12:2085–2090. CrossRef Medline
- Kuusisto E, Kauppinen T, Alafuzoff I (2008) Use of p62/SQSTM1 antibodies for neuropathological diagnosis. *Neuropathol Appl Neurobiol* 34:169–180. CrossRef Medline
- Labbadia J, Cunliffe H, Weiss A, Katsyuba E, Sathasivam K, Seredenina T, Woodman B, Moussaoui S, Frentzel S, Luthi-Carter R, Paganetti P, Bates GP (2011) Altered chromatin architecture underlies progressive impairment of the heat shock response in mouse models of Huntington disease. *J Clin Invest* 121:3306–3319. CrossRef Medline
- Labbadia J, Novoselov SS, Bett JS, Weiss A, Paganetti P, Bates GP, Cheetham ME (2012) Suppression of protein aggregation by chaperone modification of high molecular weight complexes. *Brain* 135:1180–1196. CrossRef Medline
- Lamark T, Perander M, Outzen H, Kristiansen K, Øvervatn A, Michaelsen E, Bjørkøy G, Johansen T (2003) Interaction codes within the family of mammalian Phox and Bem1p domain-containing proteins. *J Biol Chem* 278:34568–34581. CrossRef Medline
- Li M, Miwa S, Kobayashi Y, Merry DE, Yamamoto M, Tanaka F, Doyu M, Hashizume Y, Fischbeck KH, Sobue G (1998) Nuclear inclusions of the androgen receptor protein in spinal and bulbar muscular atrophy. *Ann Neurol* 44:249–254. CrossRef Medline
- Lieberman AP, Harmison G, Strand AD, Olson JM, Fischbeck KH (2002) Altered transcriptional regulation in cells expressing the expanded polyglutamine androgen receptor. *Hum Mol Genet* 11:1967–1976. CrossRef Medline
- Matsumoto G, Wada K, Okuno M, Kurosawa M, Nukina N (2011) Serine 403 phosphorylation of p62/SQSTM1 regulates selective autophagic clearance of ubiquitinated proteins. *Mol Cell* 44:279–289. CrossRef Medline
- Miyazaki Y, Adachi H, Katsuno M, Minamiyama M, Jiang YM, Huang Z, Doi H, Matsumoto S, Kondo N, Iida M, Tohnai G, Tanaka F, Muramatsu S, Sobue G (2012) Viral delivery of miR-196a ameliorates the SBMA phenotype via the silencing of CELF2. *Nat Med* 18:1136–1141. CrossRef Medline
- Mizushima N, Komatsu M (2011) Autophagy: renovation of cells and tissues. *Cell* 147:728–741. CrossRef Medline
- Mizushima N, Yoshimori T, Levine B (2010) Methods in mammalian autophagy research. *Cell* 140:313–326. CrossRef Medline
- Montie HL, Cho MS, Holder L, Liu Y, Tsvetkov AS, Finkbeiner S, Merry DE (2009) Cytoplasmic retention of polyglutamine-expanded androgen receptor ameliorates disease via autophagy in a mouse model of spinal and bulbar muscular atrophy. *Hum Mol Genet* 18:1937–1950. CrossRef Medline
- Montie HL, Pestell RG, Merry DE (2011) SIRT1 modulates aggregation and toxicity through deacetylation of the androgen receptor in cell models of SBMA. *J Neurosci* 31:17425–17436. CrossRef Medline
- Nagai Y, Inui T, Popiel HA, Fujikake N, Hasegawa K, Urade Y, Goto Y, Naiki H, Toda T (2007) A toxic monomeric conformer of the polyglutamine protein. *Nat Struct Mol Biol* 14:332–340. CrossRef Medline
- Naiki H, Nagai Y (2009) Molecular pathogenesis of protein misfolding diseases: pathological molecular environments versus quality control systems against misfolded proteins. *J Biochem* 146:751–756. CrossRef Medline
- Niwa H, Yamamura K, Miyazaki J (1991) Efficient selection for high-expression transfectants with a novel eukaryotic vector. *Gene* 108:193–199. CrossRef Medline
- Orr CR, Montie HL, Liu Y, Bolzoni E, Jenkins SC, Wilson EM, Joseph JD, McDonnell DP, Merry DE (2010) An interdomain interaction of the androgen receptor is required for its aggregation and toxicity in spinal and bulbar muscular atrophy. *J Biol Chem* 285:35567–35577. CrossRef Medline
- Palazzolo I, Stack C, Kong L, Musaro A, Adachi H, Katsuno M, Sobue G, Taylor JP, Sumner CJ, Fischbeck KH, Pennuto M (2009) Overexpression of IGF-1 in muscle attenuates disease in a mouse model of spinal and bulbar muscular atrophy. *Neuron* 63:316–328. CrossRef Medline
- Pankiv S, Clausen TH, Lamark T, Brech A, Bruun JA, Outzen H, Øvervatn A, Bjørkøy G, Johansen T (2007) p62/SQSTM1 binds directly to Atg8/LC3 to facilitate degradation of ubiquitinated protein aggregates by autophagy. *J Biol Chem* 282:24131–24145. CrossRef Medline
- Sathasivam K, Lane A, Legleiter J, Warley A, Woodman B, Finkbeiner S, Paganetti P, Muchowski PJ, Wilson S, Bates GP (2010) Identical oligomeric and fibrillar structures captured from the brains of R6/2 and knock-in mouse models of Huntington's disease. *Hum Mol Genet* 19:65–78. CrossRef Medline
- Saudou F, Finkbeiner S, Devys D, Greenberg ME (1998) Huntingtin acts in the nucleus to induce apoptosis but death does not correlate with the formation of intranuclear inclusions. *Cell* 95:55–66. CrossRef Medline
- Sobue G, Hashizume Y, Mukai E, Hirayama M, Mitsuma T, Takahashi A (1989) X-linked recessive bulbospinal neuronopathy. A clinicopathological study. *Brain* 112:209–232. CrossRef Medline
- Tokui K, Adachi H, Waza M, Katsuno M, Minamiyama M, Doi H, Tanaka K, Hamazaki J, Murata S, Tanaka F, Sobue G (2009) 17-DMAG ameliorates polyglutamine-mediated motor neuron degeneration through well-preserved proteasome function in an SBMA model mouse. *Hum Mol Genet* 18:898–910. CrossRef Medline
- Troakes C, Maekawa S, Wijesekera L, Rogelj B, Siklós L, Bell C, Smith B, Newhouse S, Vance C, Johnson L, Hortobágyi T, Shatunov A, Al-Chalabi A, Leigh N, Shaw CE, King A, Al-Sarraj S (2012) An MND/ALS phenotype associated with C9orf72 repeat expansion: abundant p62-positive, TDP-43-negative inclusions in cerebral cortex, hippocampus and cerebellum but without associated cognitive decline. *Neuropathology* 32:505–514. CrossRef Medline
- Walcott JL, Merry DE (2002) Ligand promotes intranuclear inclusions in a novel cell model of spinal and bulbar muscular atrophy. *J Biol Chem* 277:50855–50859. CrossRef Medline
- Watase K, Weeber EJ, Xu B, Antalffy B, Yuva-Paylor L, Hashimoto K, Kano M, Atkinson R, Sun Y, Armstrong DL, Sweatt JD, Orr HT, Paylor R, Zoghbi HY (2002) A long CAG repeat in the mouse Sca1 locus replicates SCA1 features and reveals the impact of protein solubility on selective neurodegeneration. *Neuron* 34:905–919. CrossRef Medline
- Waza M, Adachi H, Katsuno M, Minamiyama M, Sang C, Tanaka F, Inukai A, Doyu M, Sobue G (2005) 17-AAG, an Hsp90 inhibitor, ameliorates polyglutamine-mediated motor neuron degeneration. *Nat Med* 11:1088–1095. CrossRef Medline
- Yoo SY, Pennesi ME, Weeber EJ, Xu B, Atkinson R, Chen S, Armstrong DL, Wu SM, Sweatt JD, Zoghbi HY (2003) SCA7 knockin mice model human SCA7 and reveal gradual accumulation of mutant ataxin-7 in neurons and abnormalities in short-term plasticity. *Neuron* 37:383–401. CrossRef Medline

# *dnc-1/dynactin 1* Knockdown Disrupts Transport of Autophagosomes and Induces Motor Neuron Degeneration

Kensuke Ikenaka<sup>1</sup>, Kaori Kawai<sup>1</sup>, Masahisa Katsuno<sup>1</sup>, Zhe Huang<sup>1</sup>, Yue-Mei Jiang<sup>1</sup>, Yohei Iguchi<sup>1</sup>, Kyogo Kobayashi<sup>2</sup>, Tsubasa Kimata<sup>2</sup>, Masahiro Waza<sup>1</sup>, Fumiaki Tanaka<sup>1</sup>, Ikue Mori<sup>2</sup>, Gen Sobue<sup>1,3\*</sup>

**1** Department of Neurology, Nagoya University Graduate School of Medicine, Nagoya, Japan, **2** Group of Molecular Neurobiology, Nagoya University Graduate School of Science, Nagoya, Japan, **3** Core Research for Evolutional Science and Technology (CREST), Japan Science and Technology Agency (JST), Saitama, Japan

## Abstract

Amyotrophic lateral sclerosis (ALS) is a fatal neurodegenerative disease characterized by the progressive loss of motor neurons. We previously showed that the expression of dynactin 1, an axon motor protein regulating retrograde transport, is markedly reduced in spinal motor neurons of sporadic ALS patients, although the mechanisms by which decreased dynactin 1 levels cause neurodegeneration have yet to be elucidated. The accumulation of autophagosomes in degenerated motor neurons is another key pathological feature of sporadic ALS. Since autophagosomes are cargo of dynein/dynactin complexes and play a crucial role in the turnover of several organelles and proteins, we hypothesized that the quantitative loss of dynactin 1 disrupts the transport of autophagosomes and induces the degeneration of motor neuron. In the present study, we generated a *Caenorhabditis elegans* model in which the expression of DNC-1, the homolog of dynactin 1, is specifically knocked down in motor neurons. This model exhibited severe motor defects together with axonal and neuronal degeneration. We also observed impaired movement and increased number of autophagosomes in the degenerated neurons. Furthermore, the combination of rapamycin, an activator of autophagy, and trichostatin which facilitates axonal transport dramatically ameliorated the motor phenotype and axonal degeneration of this model. Thus, our results suggest that decreased expression of dynactin 1 induces motor neuron degeneration and that the transport of autophagosomes is a novel and substantial therapeutic target for motor neuron degeneration.

**Citation:** Ikenaka K, Kawai K, Katsuno M, Huang Z, Jiang Y-M, et al. (2013) *dnc-1/dynactin 1* Knockdown Disrupts Transport of Autophagosomes and Induces Motor Neuron Degeneration. PLoS ONE 8(2): e54511. doi:10.1371/journal.pone.0054511

**Editor:** Udai Pandey, Louisiana State University Health Sciences Center, United States of America

**Received:** October 2, 2012; **Accepted:** December 12, 2012; **Published:** February 7, 2013

**Copyright:** © 2013 Ikenaka et al. This is an open-access article distributed under the terms of the Creative Commons Attribution License, which permits unrestricted use, distribution, and reproduction in any medium, provided the original author and source are credited.

**Funding:** This work was supported by Grants-in-Aid for Scientific Research and Global COE Program from the Ministry of Education, Culture, Sports, Science, and Technology, Grants-in-Aid for Scientific Research from the Ministry of Health, Labor, and Welfare, a Grant-in-Aid for Scientific Research on Innovative Areas "Foundation of Synapse and Neurocircuit Pathology", and Core Research for Evolutional Science and Technology (CREST) from Japan Science and Technology Agency (JST). The funders had no role in study design, data collection and analysis, decision to publish, or preparation of the manuscript.

**Competing Interests:** The authors have declared that no competing interests exist.

\* E-mail: sobueg@med.nagoya-u.ac.jp

## Introduction

Autophagy is one of the major cellular systems that regulate protein degradation and organelle turnover in physiological and pathological conditions [1], and it is an essential quality control system for proteins in post-mitotic neurons that need to eliminate abnormal proteins and organelles for their proper function and survival [2,3]. It is well known that the dysregulation of autophagy causes neurodegeneration [4,5] and that the abnormal accumulation of autophagosomes is observed in several neurodegenerative diseases [6–9]. Particularly, intensified immunoreactivity for microtubule-associated protein 1 light chain 3 (LC3), which is a marker of autophagosome, is often observed in the spinal motor neurons of amyotrophic lateral sclerosis (ALS) patients [8,10]. Electron microscopy of the motor neurons of ALS patients shows an increased number of autophagosomes surrounded by a double-membrane that contain sequestered cytoplasmic organelles, e.g., mitochondria [8]. Although these observations suggest the possibility that autophagy is upregulated to protect neurons from increased amounts of aggregated proteins and/or damaged

organelles, it is also possible that the accumulation of autophagosomes due to dysregulated autophagy leads to neurodegeneration.

One possible mechanism for the accumulation of autophagosomes in degenerated neurons is the disruption of the cellular transport system, given that autophagosomes are cargo that moves bidirectionally along microtubules, which is powered by the kinesin family of motor proteins and dynein/dynactin complexes [11,12]. We previously investigated the motor neuron-specific gene expression profile of sporadic ALS (SALS), which accounts for more than 90% of ALS, and found that the expression of dynactin 1, which is a key member of the dynactin family, is markedly decreased in the spinal motor neurons of SALS patients [9]. The decreased expression of dynactin 1 was also verified quantitatively using *in situ* hybridization analysis of tissues from SALS patients [13]. By contrast, the expression of other motor proteins including the kinesin family, which are responsible for anterograde transport and dyneins, which are responsible for retrograde transport was not significantly changed. Thus, we hypothesized that the decreased expression of dynactin 1 results in the disrupted transport of autophagosomes and thus attenuates the protective effects of autophagy against neurodegeneration.

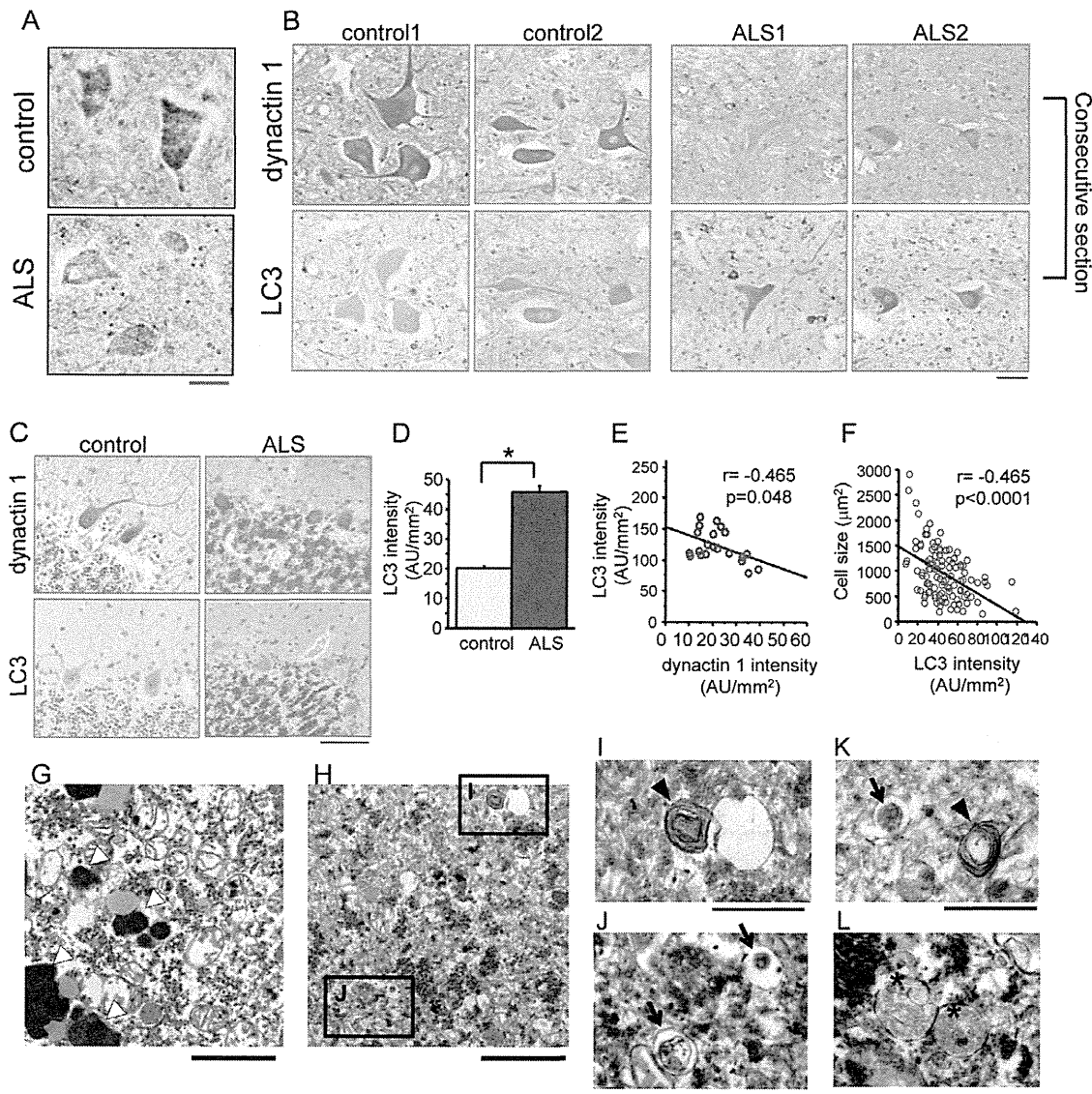


**Figure 1. Dysregulated expression of dyneactin 1 and the accumulation of autophagosomes in SALS patients.** (A) Representative *in situ* hybridization for *DCTN1* in the spinal cords of control and ALS patients. (B, C) Representative immunohistochemistry for dyneactin 1 and microtubule-associated protein 1 light chain 3 alpha (LC3) on consecutive spinal cord (B) and cerebellar (C) sections from control and ALS patients. (D) Quantification of the signal intensity of LC3 in anterior horn neurons of the spinal cord (n = 20 sections from 4 patients for each group). (E) Correlation between LC3 intensity and the expression of *DCTN1* in individual motor neurons from SALS patients (n = 12 consecutive sections from 3 SALS patients). (F) Correlation between the intensity of LC3 immunoreactivity and the size of motor neurons in SALS patients (n = 20 sections from 4 patients). (G–L) Electron microscopy images of spinal motor neurons. Representative lower magnification image of a motor neuron from a control patient (G) and lower (H) and higher magnification images (I–L) from SALS patients. The open arrowheads indicate lipofuscin. There were abundant autophagic vacuoles, e.g., multi-lamellar bodies (arrowheads in I, K), autophagosome-like double membrane vesicles (arrows in K, J), and autolysosomes (asterisks in L) in the motor neurons of SALS patients, but not of the control. Scale bar = 50 μm (A–C), 2 μm (G, H), or 1 μm (I–L). Statistical analyses were performed using Student's t test (\*p < 0.0001) and Pearson's correlation coefficient in E and F. The error bars are S.E.M. doi:10.1371/journal.pone.0054511.g001

Moreover, mutations of *DCTN1*, the gene encoding dyneactin 1, are linked to familial lower motor neuron disease [14]. Several mutant *DCTN1* models exhibited motor dysfunction and pathological changes related to motor neuron disease [15,16]. As seen in the motor neurons of SALS patients, mutant *DCTN1* mice exhibited a massive accumulation of membrane vesicles, including autophagosomes, in spinal motor neurons [16]. Although these findings suggest that impaired vesicular trafficking might cause the

accumulation of vesicles, it remains unclear whether the transport of autophagosomes is actually impaired in the mutant *DCTN1* mice or whether the accumulation of autophagosomes plays a causative role in the pathogenesis of motor neuron degeneration.

The aim of the present study was to clarify the biological link between the quantitative loss of dyneactin 1 and the disruption of autophagy. In particular, we examined whether the decreased levels of dyneactin 1 induce motor neuron degeneration by

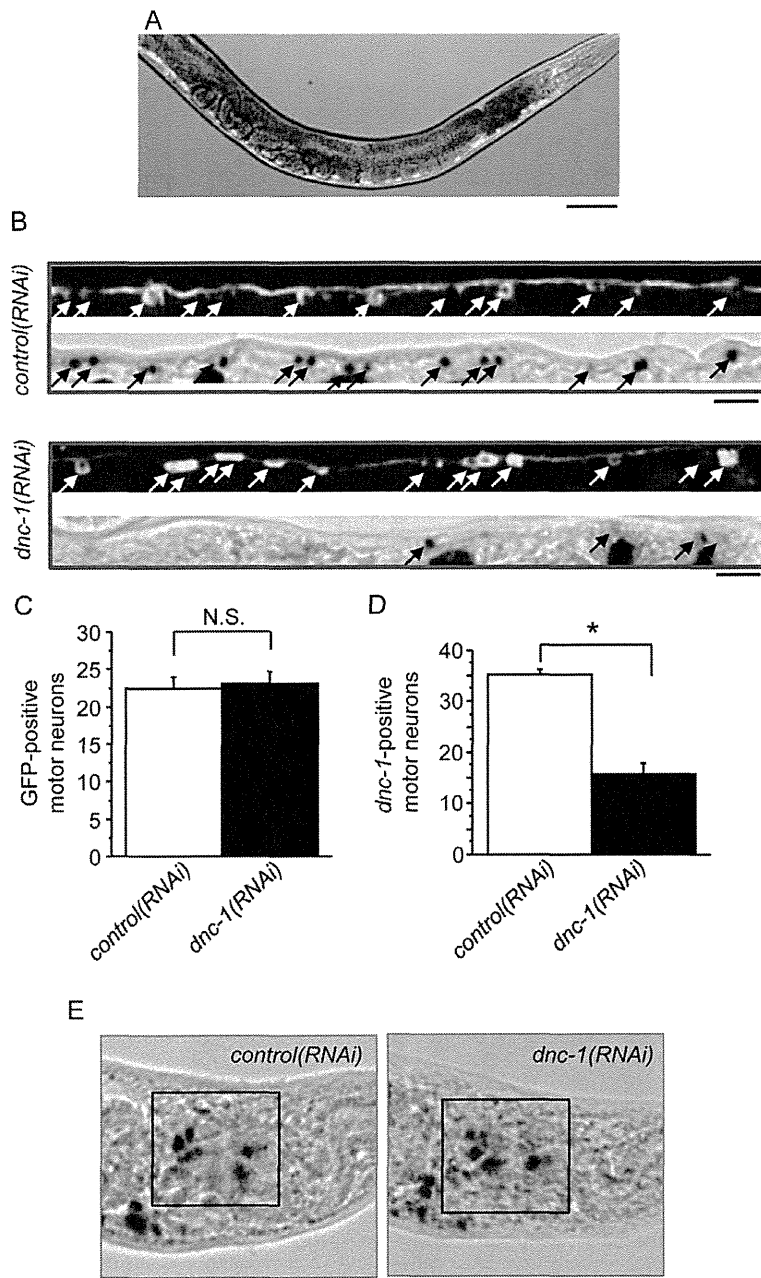


**Figure 2. Creation of the motor neuron-specific *dnc-1*-KD *C. elegans* model.** (A) Fluorescent visualization of ventral cholinergic motor neurons and their neurites in transgenic *C. elegans* worms expressing *acr2p::shRNA::gfp*. (B) Representative immunohistochemical staining of GFP and *in situ* hybridization against *dnc-1* in ventral cholinergic motor neurons and their neurites in the *control(RNAi)* and *dnc-1(RNAi)* worms. (C) The number of GFP-positive motor neurons (white arrows in B) was not significantly different between the *control(RNAi)* and *dnc-1(RNAi)* worms ( $n = 20$  animals for each strain). (D) Conversely, the number of *dnc-1* mRNA-positive neurons (black arrows in B) was remarkably decreased in the *dnc-1(RNAi)* worms ( $n = 20$  animals for each strain). (E) Representative images of *in situ* hybridization for *dnc-1* in the head neurons. Scale bars = 100  $\mu$ m (A), 10  $\mu$ m (B), and 20  $\mu$ m (E). Statistical analyses were performed using Student's t test (\* $p < 0.0001$ ). The error bars are S.E.M. doi:10.1371/journal.pone.0054511.g002

hindering the transport of autophagosomes. To this end, we first examined the relationship between the decreased levels of dynactin 1, the accumulation of autophagosomes, and motor neuron degeneration in post-mortem tissues from SALS patients. Next, we created a *Caenorhabditis elegans* (*C. elegans*) model of the motor neuron-specific knockdown (KD) of *dnc-1*, the *C. elegans*

homolog of human *DCTN1*, using small hairpin RNA (shRNA), and investigated whether the depletion of dynactin 1 impairs the transport of autophagosomes and thereby induces motor neuron degeneration. Using this model, we also explored therapeutic strategies targeting the transport of autophagosomes.

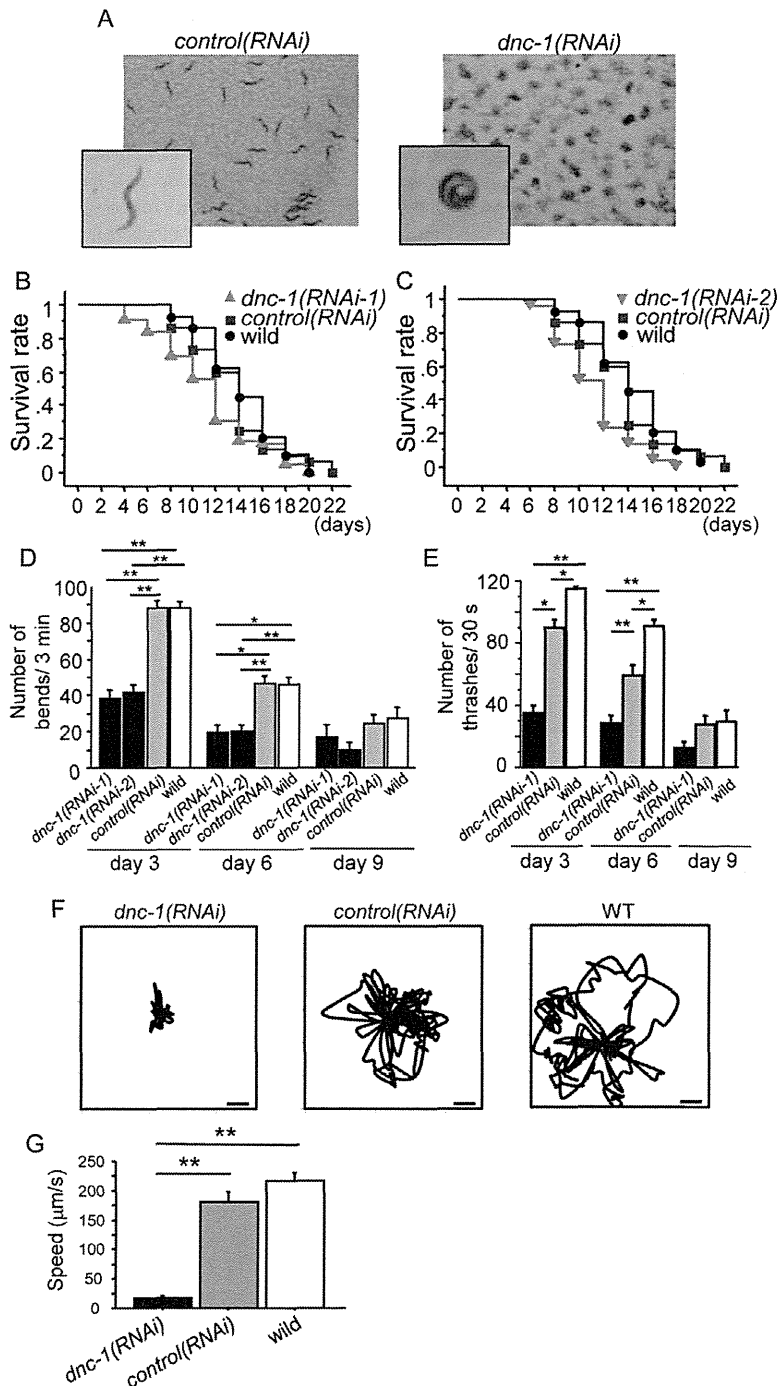


**Figure 3. Motor dysfunction in the motor neuron-specific *dnc-1*-KD *C. elegans* model.** (A) Stereoscopic microscopy showing the phenotypes of the *control(RNAi)* and *dnc-1(RNAi)* worms. (B, C) Survival curves of the transgenic worms (*dnc-1(RNAi-1)*,  $n=90$ ; *dnc-1(RNAi-2)*,  $n=90$ ; *control(RNAi)*,  $n=90$ ; and wild-type,  $n=30$ ). The same survival data of the *control(RNAi)* and wild-type worms were used in both graphs. Both *dnc-1(RNAi)* worms with different shRNA sequences (101, 2888) had significantly reduced life spans compared with the *control(RNAi)* worms (101:  $p=0.005$ ; 2888:  $p<0.0001$ ; log-rank test). (D) The number of body bends associated with forward movement in 3 min. (E) The number of thrashing movements in liquid medium in 30 s. (F, G) The tracks (F) and average speed of the worms (G) analyzed by video capture at day 4. Scale bars in F = 100  $\mu\text{m}$ . The error bars are S.E.M. ( $n=30$ , 30, 40, and 40 for *dnc-1(RNAi-1)*, *dnc-1(RNAi-2)*, *control(RNAi)*, and wild-type, respectively, in D, E; and  $n=6$ , 6, and 6 for *dnc-1(RNAi-1)*, *control(RNAi)*, and wild-type, respectively, in G). The statistical analyses in C, D, and F were performed by one-way ANOVA followed by the Bonferroni/Dunn post hoc test (\* $p<0.001$  and \*\* $p<0.0001$ ). doi:10.1371/journal.pone.0054511.g003

## Materials and Methods

### Protocols for the human samples

**Ethics Statement.** The collection of autopsied human tissues and their use for this study were approved by the Ethics Committee of Nagoya University Graduate School of Medicine, and written informed consent was obtained from the patients' next-of-kin. Experimental procedures involving human subjects were conducted in conformance with the principles expressed in the Declaration of Helsinki.

**Immunohistochemistry.** Six micrometer-thick sections from paraffin-embedded spinal cord sections from autopsied patients were prepared as described previously [17]: four patients with sporadic ALS ( $64.5 \pm 9.3$  years-old; M:F = 2:2) and four disease controls ( $73.5 \pm 5.4$  years-old; M:F = 1:3). The four control patients were diagnosed with progressive supranuclear palsy, multiple system atrophy, diffuse lewy body disease, and Parkinson's disease, respectively. The sections were first microwaved for 20 min in 50 mM citrate buffer, pH 6.0, then blocked with TNB blocking buffer (PerkinElmer, Hvidovre, Denmark) in Tris-

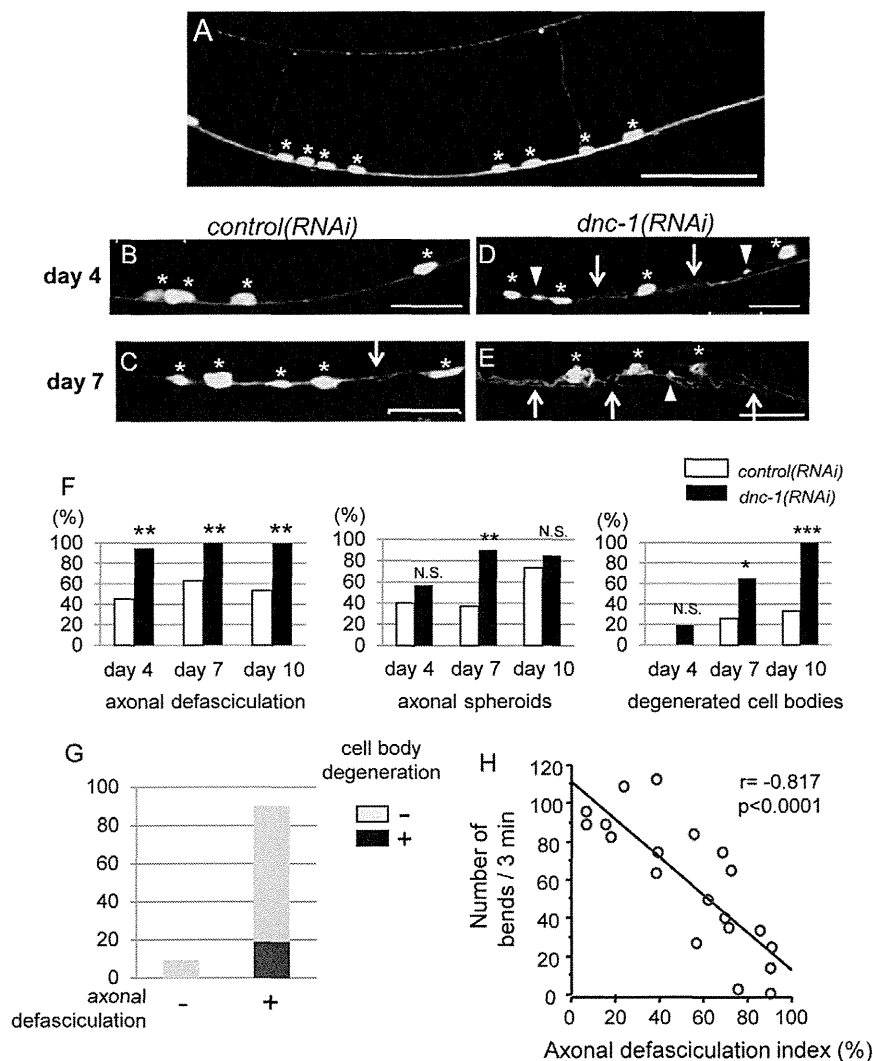


**Figure 4. Morphological changes in ventral motor neurons.** (A) Representative view of fluorescent GFP microscopic images of the ventral nerve cord in a *control(RNAi)* *C. elegans*. All of the motor neurons (white asterisks) were located in the ventral side of the worm. Axons from the motor neurons project within the ventral nerve cord or toward the dorsal side. (B–E) Representative view of the ventral nerve cord in the *control(RNAi)* worms (B, C) and *dnc-1(RNAi)* worms (D, E). The degenerated axons were defasciculated (arrows in D, E) and formed spheroids (arrowheads in D, E) in the *dnc-1(RNAi)* worms. Mild defasciculation was observed occasionally in the *control(RNAi)* worms (arrow in C). While the cell bodies of the motor neurons were regular and round in *control(RNAi)* and young adult *dnc-1(RNAi)* worms (white asterisks in B–D), abnormally shaped cell bodies (yellow asterisks in E) were observed only in the worms with severe axonal changes. (F) Semi-quantification of the abnormal morphological changes in the *control(RNAi)* and *dnc-1(RNAi)* worms. The percentage of worms with axonal defasciculation, axonal spheroids, or cell body degeneration on days 4, 7, and 10. (G) Population of *dnc-1(RNAi)* worms with and without cell body degeneration (black and gray boxes, respectively) on day 4. (H) Correlation between the axonal defasciculation index and locomotor function in the *dnc-1(RNAi)* worms. The axonal defasciculation index represents the degree of axonal defasciculation (its details are described in the Materials and Methods). Scale bars = 20  $\mu$ m. The statistical analysis in F was performed using Fisher's exact probability test (\* $p < 0.05$ , \*\* $p < 0.001$ , and \*\*\* $p < 0.0001$ ) and Pearson's correlation coefficient in H.

doi:10.1371/journal.pone.0054511.g004